Size Resolved Aerosol Characterization and In-field Comparative Evaluation of TSI 1 nm SMPS at Lake Michigan Coastal Station

Megan B. Christiansen[1*], Charles O. Stanier[1], Dagen D. Hughes[2], Elizabeth A. Stone[1,2], R. Bradley Pierce[3], Sherrie Elzey[4]

[1]Department of Chemical and Biochemical Engineering, University of Iowa, Iowa City, Iowa, United States of America

[2]Department of Chemistry, University of Iowa, Iowa City, Iowa, United States of America

[3]Space Science and Engineering Center, University of Wisconsin-Madison, Madison, Wisconsin, United States of America

[4]TSI Incorporated, Shoreview, Minnesota, United States of America

*Corresponding Author e-mail: megan-christiansen@uiowa.edu

Abstract

The atmospheric particle size distribution was measured at a rural lakeshore site (Zion, IL 42.468 N, 87.810 W) during the Lake Michigan Ozone Study (LMOS 2017) in May and June 2017. The full aerosol size distribution was continuously measured by two scanning mobility particle sizers and an aerodynamic particle sizer in the range of 1.02 to 8671 nm (electrical mobility diameter). The Zion site, 0.5 km from the lake, was one of two enhanced monitoring ground stations with collocated meteorology, remote sensing platforms, gravimetric filters, and gas-phase variables. Quantified size distributions of aerosols are important for understanding aerosol climate and health effects, for evaluation of models, and for understanding aerosol sources. Few studies have provided continuous, highly time-resolved, full particle size distribution near the shore of Lake Michigan, and none prior to this have extended measurements into the 1-3 nm size range. There were 14 identified ultrafine burst events, defined as particle growth from sub 10 nm to 25-100 nm, and all events began in the morning hours. Lake spray aerosol was investigated on June 5 when wave breaking conditions were sustained over the lake. The number distribution mode was 81 nm during the event; however, the amplitude of the particle size distribution dropped from 9000 cm^{-3} prior to the onset to 3000 cm^{-3} during and post event. Additional wind speed and direction analysis resulted in no identifiable pattern in the ultrafine particles when wind velocity exceed 4 m/s. Other measurement highlights include the mean number concentrations for 1-3 nm and 3-8761 nm were 1.80×10^4 cm^{-3} and 7998 cm^{-3} respectively, aerosol optical depth (0.084), reconstructed $PM_{2.5}$ (6.4 μg m^{-3}), reconstructed PM_{10} (7.9 μg m^{-3}) and SO_2 (0.32 ppb). Implications for future air quality management are also discussed.

Introduction

Aerosols play an important role in the effects of air pollution on human health, cloud interactions, and climate change. Aerosols have direct effects on the climate (e.g. scattering and absorbing solar radiation) and indirect effects through cloud microphysics and albedo [1, 2]. Aerosols classified as fine particulate matter ($PM_{2.5}$; aerosols ≤ 2.5 μm aerodynamic diameter) are a concern to the human population sensitive to respiratory illnesses because of their ability to deposit in the airways and lungs [3, 4]. Thus, $PM_{2.5}$ is a criteria air pollutant monitored and regulated by the Environmental Protection Agency (EPA) through the National Ambient Air Quality Standards (NAAQS). However, many climate and health effects of aerosol particles are strongly influenced by particle size; thus, measurement of aerosol size distribution in concert with metrics such as $PM_{2.5}$ gives a much more complete picture of aerosol processes. For example, ultrafine aerosol particles (with diameters less than 100 nm) account for a significant fraction of inhaled aerosols, particularly if the respirable dose is weighted by particle number or surface area [5, 6]. These aerosols have very little volume or mass and are therefore missed by measuring solely $PM_{2.5}$ concentrations.

The Lake Michigan Ozone Study 2017 (LMOS 2017) was a multi-site collaborative field campaign developed to gather high spatio-temporal resolution data in support of ongoing efforts for improvement of regional air quality [7]. The campaign provided extensive observational datasets regarding ozone, its precursors, particulate matter, and meteorology associated with ozone events through a combination of airborne, ship, mobile lab, and fixed ground-based sites. The overarching goal of LMOS was to investigate ozone formation and transport; aerosol measurements during LMOS were conducted to support source apportionment and site characterization. Photochemical Grid Models (PGM) were used for forecasting and post-

campaign analysis, and ground-based, aircraft, and satellite remote sensing products have been integrated into LMOS analyses.

During LMOS 2017, aerosol measurements were conducted primarily at the Zion, IL ground site, 67 km north of Chicago. This paper builds on previous publications that have discussed aerosol and particle-phase measurements from Zion. Mean daytime particle number (5711 cm^{-3}), $PM_{2.5}$ (6.4 µg m^{-3}), and PM_{10} (8.3 µg m^{-3}) were reported in Doak et al. [8] together with a comprehensive site characterization for Zion. Doak et al. [8] also used particle size distribution measurements to quantify enhancement in ultrafine particles within a few minutes of passage of diesel locomotives, on the rail line 0.54 km from the site. Hughes et al. [9] reported $PM_{2.5}$ speciation, dominated by organic matter (average of 59%), and showed significant variation in chemical composition and regional origin of $PM_{2.5}$ during each of the three high ozone event periods. Wagner et al. [10] presented detailed characterization of the lake breeze behavior during LMOS 2017, quantifying the well-known sharp changes in wind direction, temperature, water vapor, and stability at time of lake breeze arrival. Furthermore, Wagner et al. [10] showed that lake breeze arrival was also associated with a sudden and statistically significant increase in the ultrafine aerosols, and with gradual increases in $PM_{2.5}$ and aerosol backscatter following lake breeze arrival [10].

Previous studies deployed impactors to study aerosol size distribution and composition around the Great Lakes. During the LMOS 1991 field campaign, the Lake Michigan Urban Air Toxics Study (LMUATS) measured several aerosol air toxin species at a ground station in downtown Chicago and aboard a research vessel stationed offshore of Chicago on Lake Michigan [11]. The Atmospheric Exchange over Lakes and Oceans (AEOLOS) occurred during July 1994 and January 1995 in urban Chicago, IL and over southern Lake Michigan [12]. In

these studies, the focus was better understanding of the atmospheric toxic chemicals and trace metals that affect the Lake Michigan ecosystem. The aerosol size distributions were binned per the specific impactor instrument used and related to the specific species of interest. To the authors' knowledge a full high time-resolved aerosol size distribution near Lake Michigan has not been reported.

The lower limit of aerosol sizing instrumentation has decreased with advancements in condensation particle counter design. Widespread detection down to 3 nm was enabled by the TSI 3025 "ultrafine" condensation particle counter (CPC), which was based on the design of Stolzenburg and McMurry [13]. The lower limit of detectable size has been extended to below 2 nm using pre-growth chambers [14, 15]. Specifically, a diethylene glycol (DEG) UCPC was placed inline of a scanning mobility particle sizer (SMPS) as a "pre-growth" step, and then particles were passed a butanol CPC to further grow the particles to sizes detectable by light scattering [16]. They were able to show the instrument's viability in-field to measure nucleation events and this led to the design of the commercial 1 nm SMPS by TSI. This instrument is described further in Aerosol Size Instrumentation section of this work.

Aerosols formed from wave breaking events in high salinity bodies of water, sea spray aerosols (SSA), are large contributors to the atmospheric aerosol population [17]. During the CABINEX campaign, flight-based aerosol size distributions over Lake Michigan showed that ultrafine particles, with a mode of 30 nm, were prominent over the lake especially during time periods of high wind speeds associated with breaking waves [18]. Similarly, during LMOS 2017 a significant mode (38 nm) in the aerosol size distributions was present following lake breeze events when compared to pre lake breeze arrival [10]. Due to their important effects on climate many PGMs include SSA emission parameterizations [19-21]. However, lake spray aerosols

(LSA) have not been as well studied as SSA even though freshwater produces aerosols through similar processes as seawater, and LSA are often not considered in simulations [17, 18]. Aerosol generation studies reported different size distributions [17] and ion concentrations and composition [22] between LSA and SSA. A few modeling studies have shown that by not considering LSA emissions surface number concentrations could be under predicted by up to 20% [23], PM mass concentrations may be underestimated by 5-25% [24], and the gas-phase partitioning to particle phase [24] over the Great Lakes is affected.

While previous LMOS 2017 publications have used portions of the aerosol size distribution and particle count data measured at Zion, in this paper we present the comprehensive result of the full aerosol size distribution and its temporal variation, merged across three sizing instruments. The details of field deployment, data processing, and quality assurance of the aerosol sizing instrumentation are reported here. We compare a standard SMPS, and the novel DEG-boosted CPC / SMPS system, in their overlapping size range (12 – 32 nm). We furthermore report comparison to the independently measured particle number from a CPC, to filter-based aerosol mass, and to aerosol optical depth measured by AERONET at Zion. These are then used in conjunction with wind and wave measurements to place an upper limit on the influence of LSA during LMOS 2017. This comprehensive report and analysis of the aerosol number size distribution measured at Zion, IL during LMOS 2017 is meant to inform aerosol modeling and measurement studies motived by health and climate effects, evaluate the novel DEG-boosted CPC / SMPS, document the relationship between PM2.5 and AOD and the location, provide insight into the processes controlling the aerosol distribution, and provide a rare field assessment of the impact of LSA on ultrafine aerosols.

Methods

Campaign and Site Description

LMOS 2017 occurred May 22 to June 22 2017. The campaign employed two aircraft, ship, mobile labs, two enhanced-monitoring sites (Spaceport Sheboygan, WI and Zion, IL), and various supplemental remote sensing systems. Further details and an overview of LMOS 2017 have been described in Stanier et al. [7].

The Zion site (42.468 N, 87.810 W) was collocated with an Illinois AQS monitoring station (AQS ID 17-097-1007) inside the Illinois State Beach Park. The site is 900 m inland due west from the lake shore with an active rail line and main arterial roadway 540 m and 1.3 km due west, respectively. A detailed characterization of both ground sites can be found in Doak et al. [8]. Field access was approved by the Lake Michigan Biological Station, The Illinois Beach State Park, and the Illinois Environmental Protection Agency, which all had overlapping oversight of the field station and its supporting infrastructure (roads, power, staging of materials, etc.).

Instrumentation

Aerosol Size Instrumentation

The University of Iowa deployed several instruments during the LMOS campaign at the Zion, IL ground site to measure the full aerosol size distribution. A summary of the variables measured, time resolution, and sampling instruments are listed in Table 1 and aerosol instrument flow diagrams as in Fig 1. Three separate inlets were used for particle sizing and counting equipment.

Table 1. Zion site instrument information reported in this work.

Instrument	Measurement	Sampling Frequency
TSI 1 nm SMPS	PSD 1-32 nm	2 min
TSI Std. SMPS	PSD 12-562 nm	2 min
TSI APS 3321	PSD 542 nm – 10 µm	2 min
TSI CPC 3025	Total particle number	2 min
$PM_{2.5}$ medium-volume filter samplers	$PM_{2.5}$ mass, elemental carbon, organic carbon, inorganic ions (sodium, potassium, magnesium, calcium, ammonium, chloride, nitrite, nitrate, sulfate), select metals, molecular organic tracers	12 hr
AERONET	Aerosol optical depth	Varying

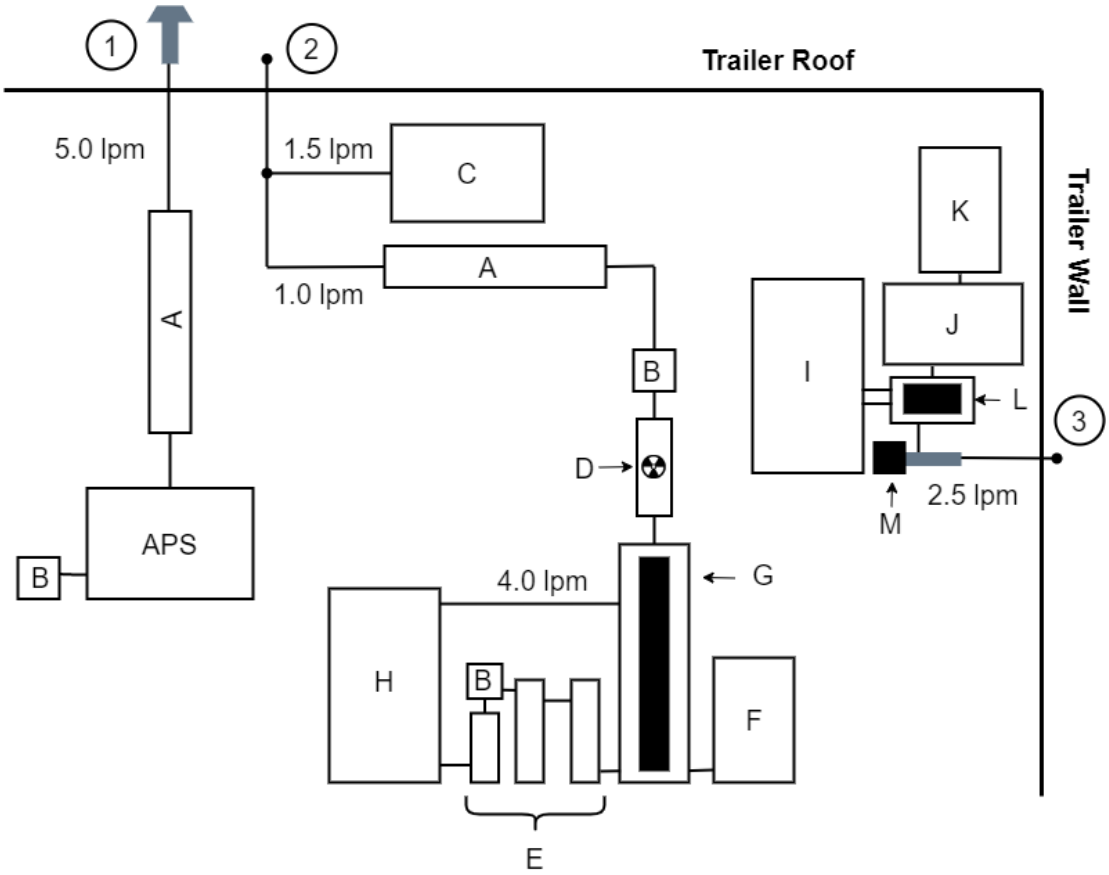

Fig 1. Aerosol instruments deployed during LMOS. Numbers refer to inlets: APS equipped with the PM_{10} inlet (1), SMPS and CPC inlet (2) and 1 nm SMPS inlet (3) consisting of bug and

rain guards. Letters refer to: diffusion dryers (A), RH sensors (B), butanol CPC 3025 (C), Kr-85 neutralizer (D), drierite tubes with HEPA filter (E), water CPC 3785 (F), long DMA 3081 (G), classifier 3080 (H), classifier 3082 (I), DEG nano enhancer 3777 (J), butanol CPC 3772 (K), 1 nm DMA 3086 (L), and soft x-ray neutralizer (M).

The first inlet, designed for high particle transmission of 1-10 μm particles, supplied an Aerodynamic Particle Sizer (APS, TSI 3321). The inlet included no bends and was dried with a diffusion dryer (TSI 3062) and equipped with a size-selective cyclonic inlet (PM_{10}, BGI). The APS reported data in channels ranging from 0.542 to 20 microns; in this work, we report results from 0.542 to 10 microns (aerodynamic diameter).

A second inlet was shared by a scanning mobility particle sizer (SMPS, TSI 3936L81) and an independent butanol condensation particle counter (CPC, TSI 3025) with a nominal 3 nm lower size cutoff for particle detection. The standard SMPS was equipped with a long DMA (TSI DMA 3081), Kr-85 neutralizer, diffusion dryer (TSI 3062), and water CPC (TSI 3785) with inlet and sheath flows of 1 and 4 LPM, respectively. The sheath air flow was further dried with inline silica gel absorbent. We report particle counts at sizes ranging from 12.2 to 552.3 nm in this work, and refer to this as the “SMPS” result.

A third inlet was used by the TSI 1 nm SMPS (TSI 3938E77), equipped with a 1 nm DMA column (TSI 3086), soft x-ray neutralizer (TSI 3088), diethylene glycol nano enhancer (TSI DEG enhancer 3777), and butanol CPC (TSI 3772) with inlet and sheath flows of 2.5 and 25 LPM, respectively. This inlet was kept short in length (15 cm) to maximize particle transmission efficiency. We report results from 1.02 to 32.0 nm in this work, and refer to this as the “1 nm SMPS” result.

Relative humidity probes (RH, Sensirion sensors, SHT75) continuously monitored the sampling lines at multiple points of the SMPS and APS instruments as noted in Fig 1.

Additional Instrumentation and Data Availability

$PM_{2.5}$ was collected by medium-volume integrated aerosol filters (3000B, URG Corporation) onto 47 mm Teflon filters at a flow rate of 90 liters per minute twice daily and the composition was analyzed post campaign by techniques described in Hughes et al. [9]. The Wisconsin Department of Natural Resources also measures $PM_{2.5}$ at Chiwaukee Prairie (AQS ID 55-059-0019) by beta attenuation monitors, located 4 km north of the Zion site. AERONET level 2 data for aerosol optical depth (AOD) and spectral deconvolution algorithm aerosol fractions were downloaded from www.aeronet.gsfc.nasa.gov/index.html. The AERONET was installed at Zion site from June 4 to June 21 2017. AOD was interpolated to 550 nm using an angstrom exponent

$$\tau_{\lambda_{550}} = \tau_{\lambda_{500}} \left(\frac{\lambda_{550}}{\lambda_{500}}\right)^{-\alpha} \quad 1)$$

where λ_{500} is wavelength at 500 nm, λ_{550} is wavelength at 550 nm, τ is AOD at the specified wavelength, and α is the angstrom exponent (440 – 870 nm) as reported by AERONET.

A complete list of campaign instrumentation is available in the supplemental information to Stanier et al. [7], with additional details for the Zion site in Doak et al. [8]. Data are available for public download at the NASA repository [25].

A dataset of estimated monthly mean $PM_{2.5}$ (V5.GL.02), with a spatial resolution of 0.01°x 0.01°, publicly available from the Atmospheric Composition Analysis Group at Washington University in St. Louis was used for discussion purposes in the Spatial Context and Air Quality

Implications (https://sites.wustl.edu/acag/datasets/surface-pm2-5/#versioninfo). The methods of estimation are detailed in van Donkelaar et al. [26].

The Wilmette Buoy, IL (Station 45174; 42.135 N, 87.655 W) is located 7.5 km offshore of Glencoe, IL and 39 km southeast of Zion site. The dataset was downloaded from the National Data Buoy Center (https://www.ndbc.noaa.gov/historical_data.shtml).

Data Quality Assurance and Analysis

Routine flow rates and leak checks on each aerosol instrument were performed every 3 days and following each exchange of silica absorbent. When the RH values exceeded 50% (dryers on aerosol inlets) or 20% (drierite tubes on the SMPS recirculating sheath flow), fresh absorbent was exchanged in. Daily site logs were kept for each instrument and overall site observations including current weather, activity around site, interior trailer condition, and personnel arrival and departure times.

Post campaign quality assurance consisted of flagging data using NARSTO categories (S1 Table) [27]. This included periods of known invalid data such as in-field instrument downtime, visual inspection for physically unrealistic data, and visual inspection for exceptional events that coincided with daily site logs. The SMPS was tested with certified polystyrene latex spheres (100 nm PSL spheres, Applied Physics Inc.) to ensure the accuracy of the particle size measurements of the SMPS. The particle size distributions were adjusted for diffusional, inertial, and gravitational losses by calculating transmission efficiency curves (Fig 2) for each instruments' respective inlet [27]. The 1 nm SMPS curve (blue line, Fig 2) includes corrections for the neutralizer and instrument diffusional losses. The APS particle diameters were shifted from aerodynamic diameter to electrical mobility diameter by equation 1 [28]

$$D_p = D_a\sqrt{\chi\frac{\rho_o}{\rho_p}} \qquad 2)$$

where D_p is the electrical mobility diameter, D_a is the aerodynamic diameter, ρ_o is the reference density (1.0 g cm^{-3}), χ is the shape factor, and ρ_p is the calculated particle density.

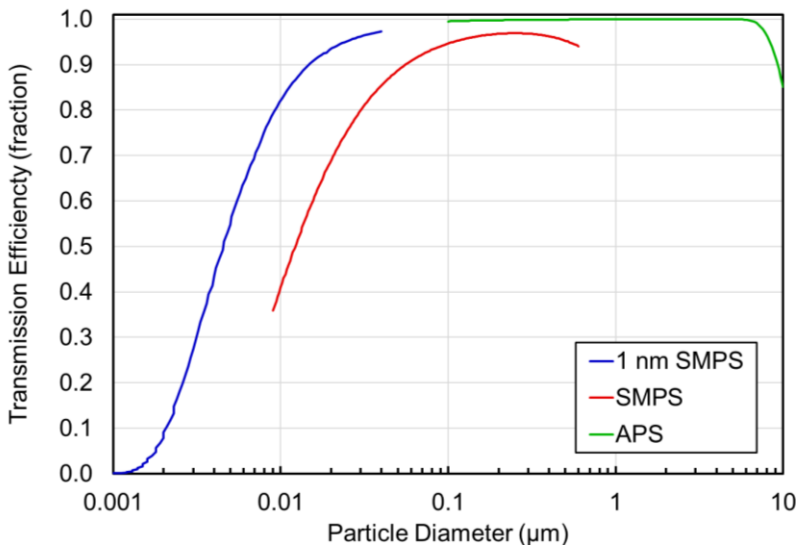

Fig 2. Aerosol transmission efficiency curves, corrected for sampling inlets, for the APS (green), SMPS (blue), and 1 nm SMPS (red) where the x-axis is in logarithmic scale. The 1 nm SMPS curve includes neutralizer and instrumental losses.

The three instruments' distributions were merged to create the overall size distribution for the entire campaign. In the overlap range between 12 and 32 nm, the SMPS was given preference, because a) the SMPS was subjected to post campaign QA/QC checks at the University of Iowa, including monodisperse PSL spheres while the 1 nm SMPS was not and b) this facilitated comparison to previous Midwestern field deployments of the SMPS [29-31]. When the SMPS was not available, the 1 nm SMPS was used in this size range. In the SMPS-

APS overlap region, the two instruments were averaged. The merged distribution is referred to hereafter as the particle size distribution (PSD).

Due to variation in instrument uptime across the three sizing instruments, there existed periods where the full merged size distribution (1.02 to 8671 nm) had missing sections. For example, if the APS was down, the size distribution was only available from 1.02 to 562 nm. In such cases, imputation was done to fill missing portions of the size distribution. Imputation was only used to fill in portions of the distribution that were low (i.e., the APS contribution to number, or the 1-nm SMPS contribution to volume). The two-step procedure for this was as follows. In step 1 of the procedure, for each 2-minute time period with any data gap, a distribution of possible gap-filled values was created using the ratio

$$P_i = P_{n,j} + P_{x,i} \qquad 3)$$

$$P_{x,i} = \frac{P_{n,i} * P_{x,j}}{P_{n,j}} \qquad 4)$$

where P is the statistic (number, surface area, volume) in question, i is the time period of the gap, j is the time index of a distribution with no missing data, x refers to bins without data for hour i, and n refers to bins where data is present for hour i. There were 5000 values in the distribution, corresponding to 5000 2-min periods with no missing data (167 hours). In step 2, the median of the distribution of P_i values was used as the gap-filled value if two tests were met. The first test was that the new (gap-filled) value did not increase relative to the non-gap-filled value by more than 5%. The second was that the coefficient of variation of the distribution of the 5000 possible gap-filled values (P_i) was small (less than 0.03). The first test made sure that the influence of imputation on the overall statistic (number, surface area, volume) was minor. The second test

rejected cases for which the size distribution in the missing bins varied considerably in time, making the gap filling uncertain.

Results

Particle Density

Particle density is required for shifting between mobility and aerodynamic diameters (equation 2). Density is also used to convert from the measured volume distribution to particle mass for intercomparison to filter-based mass from Hughes et al. [9] and to AQS network measurements, which were done at nearby sites via beta attenuation monitoring. A density of 1.33 g cm^{-3} was used. That was based on particle composition as reported in Hughes et al. [9] with densities of the major aerosol components as in Lee et al. [32]. Ammonium, nitrate, sulfate, and organic matter made up 87% of the $PM_{2.5}$ mass on average. The ammonium nitrate (AN, ρ = 1.72 g cm^{-3}), ammonium sulfate (AS, ρ = 1.79 g cm^{-3}), and organic material (OM, ρ = 1.2 g cm^{-3}) were present at relative mass fractions of 0.06, 0.25, and 0.69, respectively. A shape factor of 1 was assumed.

Particle Number Time Series

While the campaign started on May 22, the stand-alone CPC began operation on June 1. Therefore, for June 1 – June 22, 2017, the total number concentration from the stand-alone CPC can be compared to the total number from the PSD. The statistics for the entire campaign (May 22 – June 22, 2017) can be found in S2 Table. For the purpose of comparison to the CPC, the values discussed in this section are June 1 – 22, 2017. The comparison is shown as a time series and scatterplot in Fig 3 (after 2-minute averaging and synchronization to a common time basis). We used the size range from 3-8671 nm, excluding particles below 3 nm, as the CPC 3025 has a nominal lower size limit of 3 nm. The means were 8485 and 5783 cm^{-3}, respectively, for the PSD

and particle counter methods. They were highly correlated (Pearson R = 0.90) with index of agreement of 0.83 (Fig 4). One possible explanation for the discrepancy is that the PSD was adjusted to account for particle losses within the inlets of the three instruments where the CPC number concentration was not adjusted. However, the overall agreement between the independent measurements of number concentrations is a strong support of the quality assurance results and indicates that periods of non-physical high or low counts (e.g. HEPA filtration checks) have been appropriately removed from the datasets.

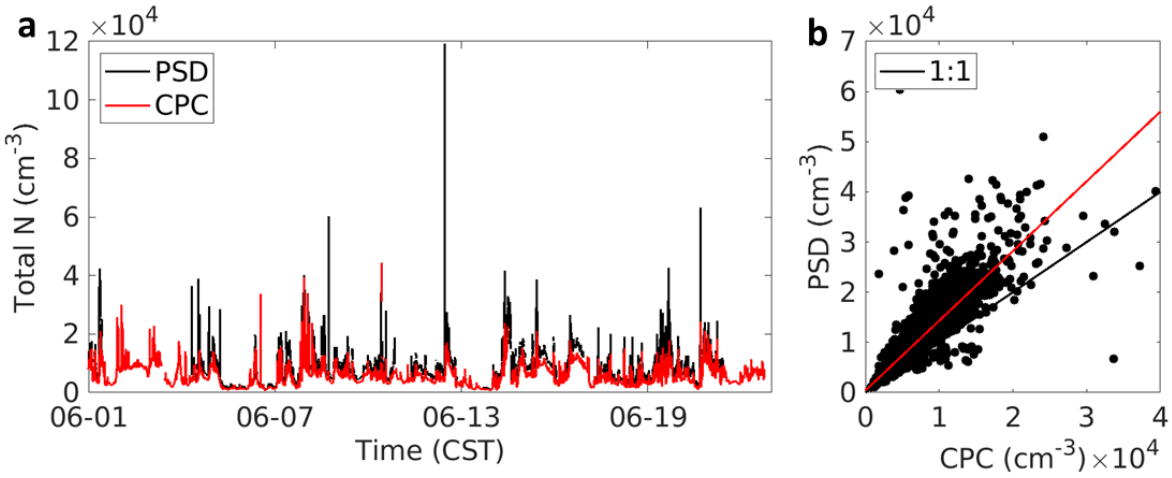

Fig 3. Timeseries (a) of CPC (red) and PSD (black) and resulting scatter plot (b) of 2 min data from June 1 – June 22, 2017. Instrument size cutoffs and loss corrections as reported in text.

Particle Size Distribution

The grand average size distributions measured during LMOS 2017 are shown in Fig 5. The number distribution was unimodal with a mode at 40 nm. The surface area and volume distributions were bimodal. The modes of the surface area distribution were at 173 nm and 2.22 µm, respectively. The modes of the volume distribution were at 223 nm and 2.66 µm, respectively. The first modes of both moments are within the accumulation mode and the second

modes are in the coarse mode. Similar distributions have been measured at other rural sites with urban impacts such as Bondville, IL [33]. The mean number concentration, $N_{3\text{-}2500}$, was higher at Zion (7993 cm^{-3}) than at Bondville (6500 cm^{-3}).

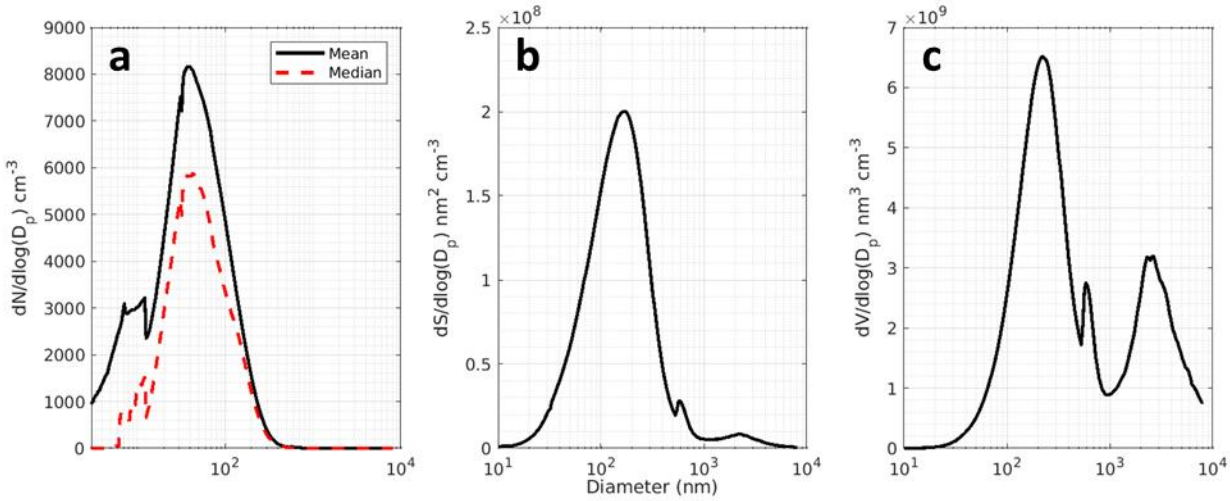

Fig 4. Arithmetic mean of number (a), surface area (b), and volume (c) distributions for the entire campaign period. Solid lines are means and the dashed line is the number distribution median. Calculations of surface area and volume based on a spherical particle assumption.

In all three distributions the modal median diameters were very similar to the mean diameters. The small size of number distribution mode suggests an influence of primary sources and secondary aerosol formation [34]. Discontinuities at 32 nm in the number distribution are due mainly to the different instrument uptime of the 1 nm SMPS and the SMPS. The discontinuity at (560 nm) in the surface and volume distribution reflect different instrument uptime of the SMPS and APS, as well as differences in measured size distribution intensity at the overlap sizes. Fine particles also dominated the collocated AERONET AOD measurements with an average fine mode fraction from Level 2 data of 0.72.

Reconstructed PM Mass from the Particle Size Distribution

The Chiwaukee Prairie and integrated filter datasets on particle mass were compared to the $PM_{2.5}$ mass reconstructed from the merged PSD together with the aerosol density assumption. Agreement provides an additional quality assurance check on these measurements. The PM_{10} concentration average was 7.9 μg m^{-3} and $PM_{2.5}$ averages for the LMOS 2017 campaign period were 5.2, 6.4, and 6.0 μg m^{-3} for the filters, reconstructed $PM_{2.5}$, and Chiwaukee Prairie, respectively. The calculated $PM_{2.5}$ and Chiwaukee Prairie site were averaged to 12 hr and any period missing more than 50% of the PSD was excluded. On average the reconstructed mass was higher than that on the filters, but well within expected uncertainty ranges given uncertainties in particle shape, density, potential artifacts in mass-based techniques, and differences in aerosol water influences.

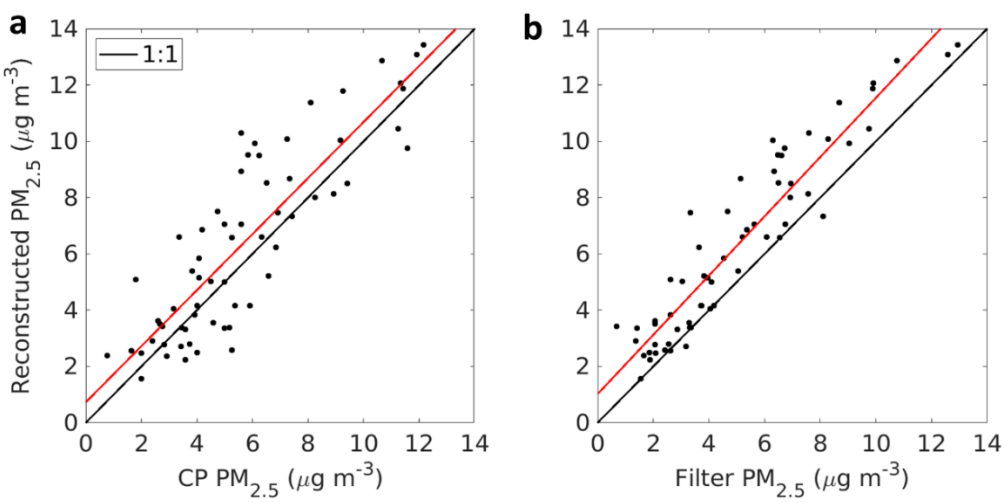

Fig 5. Reconstructed $PM_{2.5}$ at Zion compared to (a) Chiwaukee Prairie BAMS, and (b) Zion gravimetric filters. Black lines are 1:1 and red lines are linear regression.

The scatter plots (Fig 5) show the overall agreement is high for the reconstructed $PM_{2.5}$ when compared to Chiwaukee Prairie and the filters with correlation coefficients (R) of 0.86 and 0.94 respectively. Decreased correlation relative to Chiwaukee Prairie is expected due to the 4

km separation distance, and the likelihood of different local sources and slightly different impacts of from regional transport.

Mass and Aerosol Optical Depth Temporal Variation

The variation in reconstructed $PM_{2.5}$ and PM_{10} mass is shown in Fig 6 for the period June 1 to June 21. This is shown along with the Level 2 AOD recorded by the AERONET station deployed at Zion during the field campaign. Expanded figures showing pollutant variation during these three weeks, with additional pollutants graphed, are in supplemental material.

Rapid drops in $PM_{2.5}$ and PM_{10} can be seen on June 16 and June 21, where PM drops from above 10 μg m^{-3} to below 5 μg m^{-3} in just a few minutes, due to a change in air mass. The AOD at 380 nm (mean of 0.155) is considerably higher than the AOD at 550 nm (mean of 0.084), consistent with a fine-mode dominated aerosol size distribution. Temporal gaps in the AOD are due to AOD only being reported during cloud-free daylight hours.

Periods of elevated $PM_{2.5}$ (above about 15 μg m^{-3}) with AERONET AOD were captured on June 9 and June 12. The period with highest AOD (June 13) did not have APS measurements necessary for a reconstructed mass. Several hours of June 13 are also not available from the $PM_{2.5}$ recorded at Chiwaukee Prairie. The cloud screening techniques used for level 2 AOD data can be contaminated by fair weather cirrus clouds. GOES-R retrievals showed cirrus cloud over Zion during the time periods of AOD > 0.3 on June 13. Therefore, they have been excluded in the regression of Fig 7. In Figs 7 and 8 these two data points have been highlighted in red. The $PM_{2.5}/AOD_{550}$ ratio was 82.4 with a correlation R of 0.69.

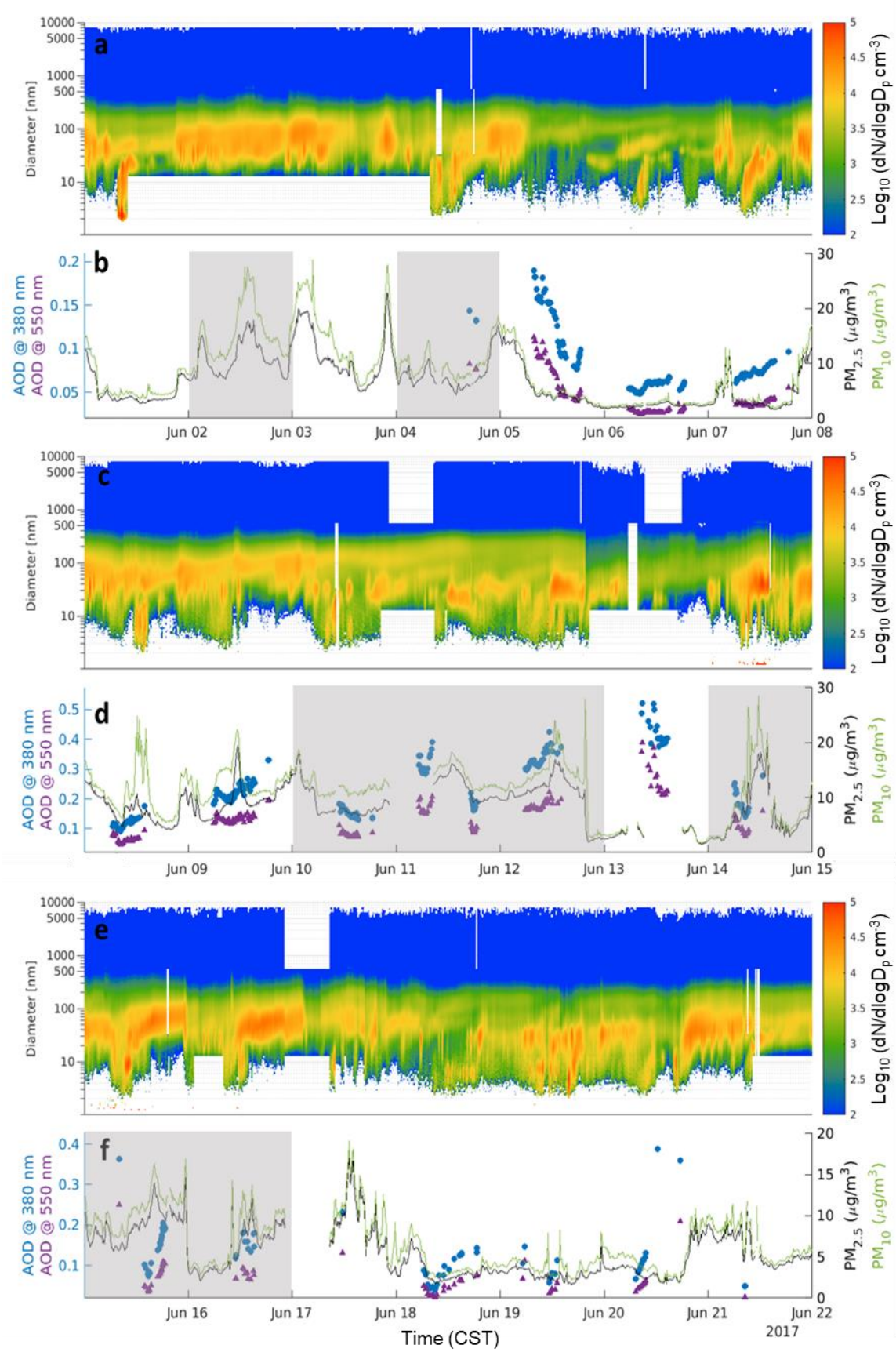
a
b
c
d
e
f
Diameter [nm]
Log10 (dN/dlogDp cm-3)
AOD @ 380 nm
AOD @ 550 nm
PM2.5 (μg/m3)
PM10 (μg/m3)
Jun 02
Jun 03
Jun 04
Jun 05
Jun 06
Jun 07
Jun 08
Jun 09
Jun 10
Jun 11
Jun 12
Jun 13
Jun 14
Jun 15
Jun 16
Jun 17
Jun 18
Jun 19
Jun 20
Jun 21
Jun 22
2017
Time (CST)

363

Fig 6. Selected aerosol variables for June 1-7 (a and b), June 8-14 (c and d), and June 15-21 (e and f) averaged to 10 min. The time series of the aerosol number size distribution is shown in panels a, c, and e. The time series of reconstructed $PM_{2.5}$ and PM_{10} mass, and AOD at 380 and 550 nm, are shown in panels b, d, and f. Gray shaded regions represent high ozone event periods.

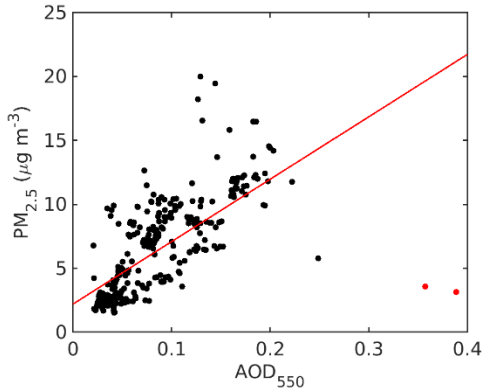

Fig 7. AOD_{550} compared to 2 min averages of the reconstructed $PM_{2.5}$. The linear regression line (red) was calculated excluding the June 13 data (red dots) due to likely cirrus contamination.

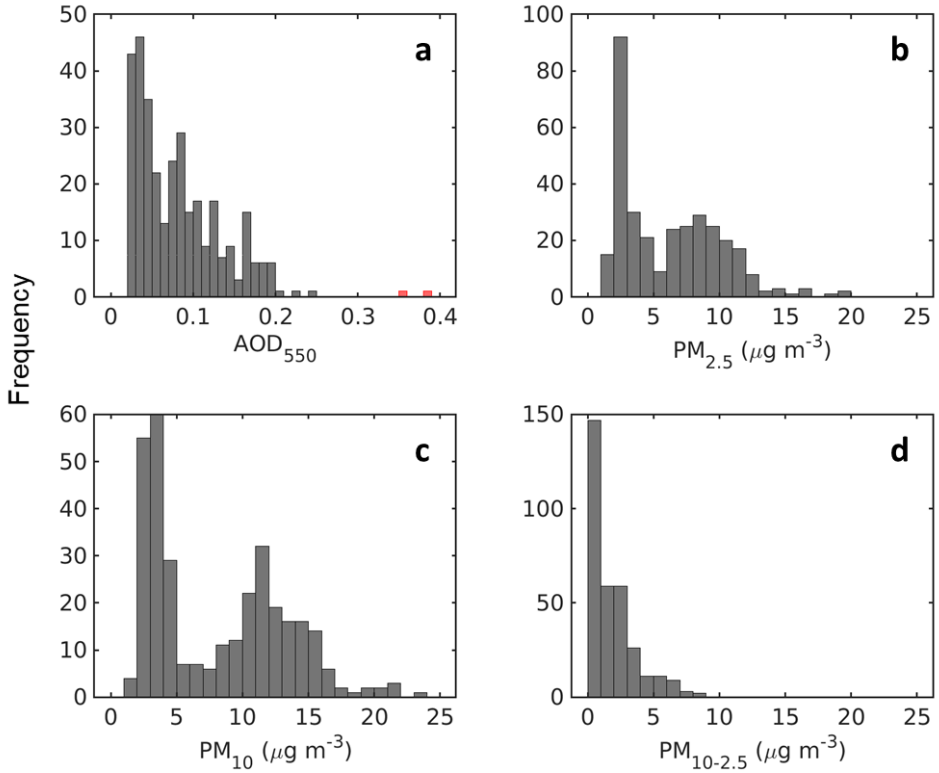

Fig 8. AOD_{550} (a), $PM_{2.5}$ (b), PM_{10} (c), and PM_{coarse} (d) (histograms) where the PM measurements are the 2 min averages that coincide with each AOD measurement. The red bars in (a) coincide with observations on June 13 that were excluded.

Inter-comparison of 1 nm SMPS and standard SMPS

The 1 nm SMPS and standard SMPS overlapped in the 12—32 nm size range. Examining this overlap is important for quality assurance and agreement between the two instruments. This region was divided into five size ranges and correlation between the two instruments was examined within each size range. The entire overlap region had a correlation coefficient (R) of 0.90 (Fig 9a). The most correlated size range was 20-24 nm (R = 0.93, Fig 10d). The least correlated size range was at the small end of the overlap region, 12-16 nm, with R of 0.82 (Fig 9b). Agreement (low mean difference) was best at the large sizes of the overlap. The mean response diverged with decreasing size, to about a 5:1 difference in the 12-16 nm size range. In other words, under 20 nm the 1 nm SMPS consistently measured higher number concentrations.

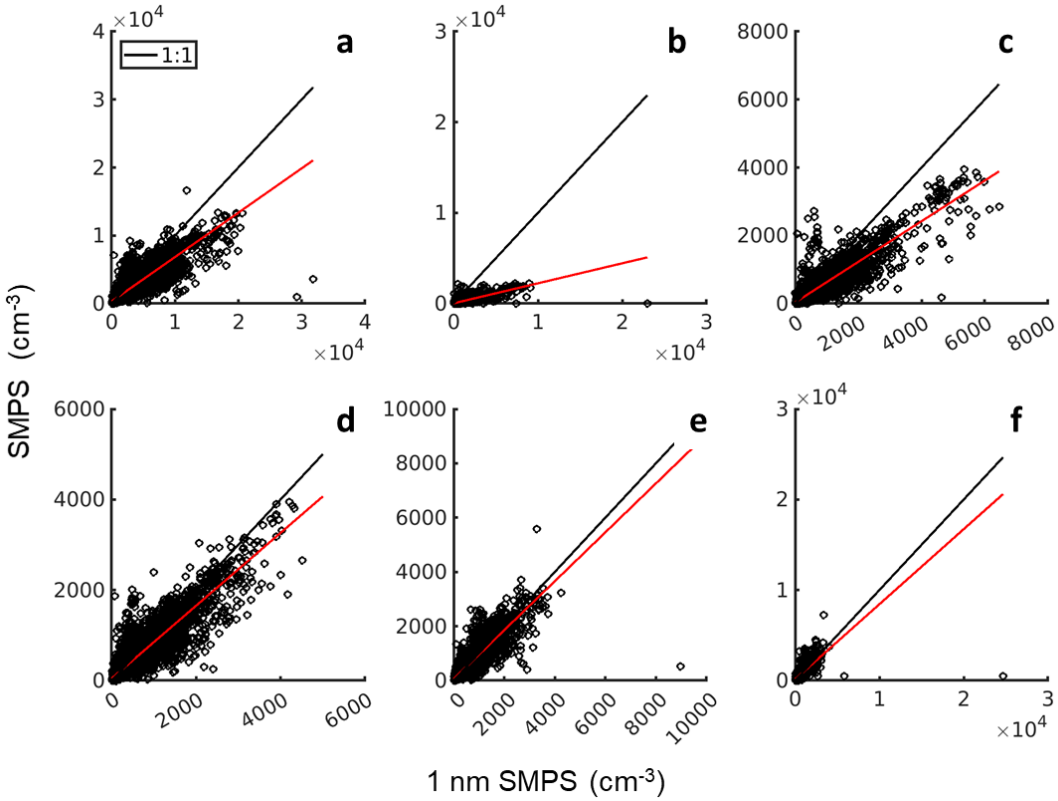

Fig 9. Scatter plots of the number concentrations in each bin of the overlap regions between the two SMPS instruments (a) 12-32 nm, (b) 12-16 nm, (c) 16-20 nm, (d) 20-24 nm, (e) 24-28 nm, and (f) 28-32 nm. Black lines are 1:1 and red lines are linear regression.

Several factors could contribute to this difference between the instruments. These include (a) the 1-nm SMPS was not dried while the SMPS aerosol and sheath air was dried; (b) the instruments had different inlets, separated by about 4 meters, and at different elevations relative to the ground; (c) the transmission efficiencies used in data processing are uncertain; (d) the difference in internal design and rod charge between the 1 nm and long DMA; and (e) the aerosol-to-sheath flow ratio influences the transmission resolution. The model 3086 1 nm DMA internal design has been optimized to reduce diffusion losses for particles <20 nm and increase the aerosol flow, and has a positively charged center rod while the long DMA is a negatively

charged rod [35]. Intercomparison of the total (neutral plus charged) size distribution is contingent on the charging assumptions used in inversions (TSI inversion was used for both the 1-nm SMPS and the SMPS). The SMPS had an aerosol-to-sheath flow ratio of 1:4 compared to the 1 nm SMPS ratio 1:10. The lower resolution ratio of the SMPS could lead to broadened transmission peaks and become more apparent in the narrow size bins of 4 nm.

New Particle Formation / Ultrafine Burst Events

Sub-10 nm particles were surprisingly low in number at the site. For example, Bullard et al. [33] reported 1755 cm^{-3} in the 3-10 nm size range in rural Illinois, driven by H_2SO_4 and organic new particle formation and growth events. These were most pronounced in spring (April) and fall (September), but there was activity in the 3-10 nm size range in late spring and early summer as well.

The mean number concentrations from 3 – 10 nm, $N_{3\text{-}10}$, were 1755 cm^{-3} and 1108 cm^{-3} for Bondville and Zion, respectively. The principal difference between these two sites is the occurrence of more intense and frequent new particle formation at Bondville. Bondville values are a grand average over 10 months. A comparison specifically for June is not possible as Bondville was a 10-month study that excluded June. However, May and July were among the four months with the highest mean number concentrations at Bondville [33]. Another possible reason is SO_2 as a factor in nucleation and growth from sulfuric acid. Zion SO_2 average was 0.32 ppb while Bondville was 0.87 ppb.

The mean number concentration from 1 – 3 nm, $N_{1\text{-}3}$, was 1.80×10^4 cm^{-3} and the timeseries is shown in Fig 10. To the best of the author's knowledge, no other atmospheric size-resolved aerosol measurements have been conducted around the Great Lakes in the sub 5 nm size range for comparison. The first atmospheric measurements were collected during the 2011

summer in Atlanta, GA with a similar diethylene (DEG) SMPS configuration [36]. Their results show number concentrations measured by the DEG SMPS are capable of reaching $1x10^7$ cm^{-3} during new particle formation events. During the PEGASOS 2012 campaign in Po Valley, Italy reported much lower overall concentrations in the 1.5 – 1.8 nm and 1.8 - 3 nm size bins, 2140 and 7980 cm^{-3} respectively, and that the majority of the clusters were electrically neutral [37]. It should be noted that the PEGASOS campaign employed different instrumentation for detection. Kangasluoma et al. [38] presents an overview of current instrumentation for sub 10 nm particle measurements and concludes that measurements are still highly uncertain in this range and additional scientific research is needed to improve the accuracy of these measurements.

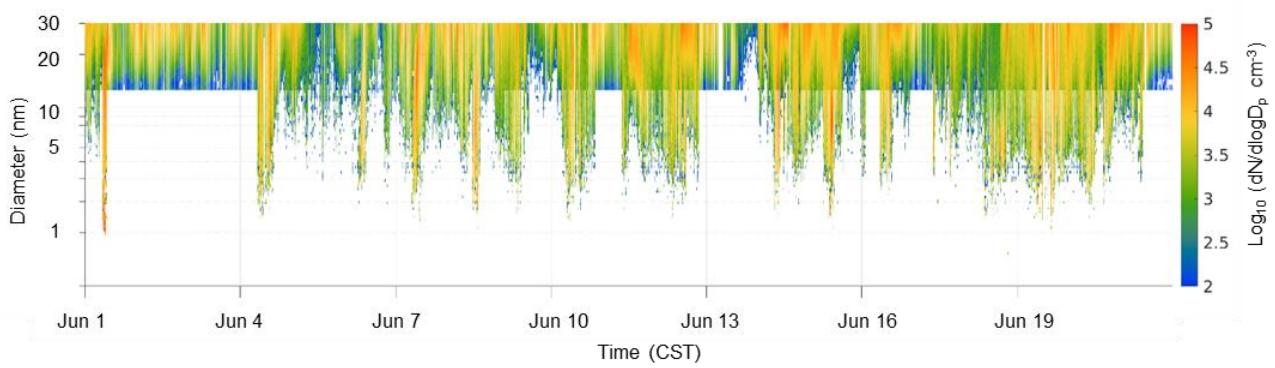

Fig 10. Number distribution from 1 to 30 nm at Zion.

Due to a combination of low concentrations and instrument uptime, few size measurements sub 10 nm occurred during the campaign and thus conventional new particle formation growth rates were not calculated. The available data allowed for the identification of 14 ultrafine burst events. These were identified qualitatively by the presence of rapid appearance of enhanced particles below 10 nm followed by growth into the 25-100 nm range visible in the size distributions [39, 40]. All events began in the morning between 10:00 am – 1:00 pm CST.

Lake Breeze and Spray Aerosol

As reported in Wagner et al. [10], lake breeze arrival corresponded to a rapid and statistically significant increase in an ultrafine mode centered at 38 nm. Furthermore, the position of the mode was consistent with observations in Slade et al. [18] who attributed the mode to LSA. The prompt timing of the enhancement with lake breeze arrival (rather than the slower buildup of ozone and $PM_{2.5}$ on lake breeze days) indicated a mechanism not tightly connected to the oxidation chemistry associated with major plumes of SOA and ozone associated with lake breeze.

In this section, we compare the microphysical aerosol measurements during LMOS 2017 to previously reported LSA aerosol studies, discuss consistency of results, and comment on three possible hypotheses for appearance of ultrafine aerosols during periods of onshore flow: (a) lake spray aerosol, (b) recent new particle formation and growth favored by chemical and meteorological features over the lake, and (c) primary particles emitted from nearby onshore sources at night, and then advected onshore in the lake breeze. Unfortunately, size-resolved chemical measurements are not available during LMOS 2017 for further interpretation; accordingly, we use the measured PSD combined with records of wind speed, wind direction, and wave height.

Prior studies of LSA can be divided into those with an ultrafine (usually number distribution) focus, and those with a focus on aerosol mass (and thus on accumulation and coarse mode particles). Both sizes are justifiable targets of study, based on prior research. Lab-generated LSA [22] has number modes at 53 and 276 nm, and a mass distribution with a mode at around 1 micron. Single particle mass spectrometry and aerosol microscopy has definitely captured the accumulation and coarse mode impacts, as reported in Axson et al. [22], May et al. [41], and Olson et al. [42]. However, ambient confirmation of the ultrafine impact beyond Slade

et al. (18) is lacking, and the magnitude of the accumulation and coarse mode impact of LSA is not well quantified.

Two prior studies are relevant for the impact of LSA on the ultrafine aerosol size distribution and total particle number, two prior studies are relevant. Slade et al. [18], reporting results of aircraft observations over northern Lake Michigan taken in 2009, reported a wind-speed dependent enhancement of particle number in the 15-40 nm size range at the lowest flight elevations; this was dependent on breaking waves. The magnitude of the enhancement was 100-400 cm^{-3} at wind speeds below 5.5 m/s, and was 1000-3000 cm^{-3} for the two flights at higher wind speeds. Chung et al. [23] simulated LSA number for summer 2004 conditions in WRF-Chem using a parameterization for wave breaking ocean aerosol. The approach relied on the weak assumption that the number of particles (but not their size or mass) is independent of water composition, such that number parameterizations for SSA can be a useful initial guess for LSA. Averaged over 2 weeks in July, particle number concentration of about 150 cm^{-3} was attributed to LSA over southern Lake Michigan, and about 100 cm^{-3} at coastal locations such as Zion. Peak periods were associated with impacts about twice the average. The simulated result was sensitive to whether new particle formation was included in the model, due to suppression of new particle formation and growth by LSA. Simulated total particle number at Zion in Chung et al. was ~12,000 cm^{-3} with new particle formation included; this is higher than the measured value at Zion (7993 $N_{3\text{-}2500}$), reflecting uncertainty in nucleation parameterizations, and decreases in nucleation precursors (e.g., SO_2) and primary ultrafine emissions between 2004 and 2017.

For larger particles, May et al. [41] sampled using a size-resolved optical particle counter and single particle mass spectrometry, 25 km downwind of Lake Michigan. The single particle signature of LSA (calcium carbonate with organics and specific ratios of cations consistent with

lake spray) was used to quantify that up to 6% of mass in the 0.5-2.0 micron size range was from LSA. This corresponded to mass and number contributions, in the 0.5-20 micron size range, of 0.2 μg m^{-3} and 0.5 cm^{-3}, respectively. Similar methods were employed on a low altitude flight on a windy day over northern Lake Michigan. There, particle counting indicated intensity of the size distribution function (dN/dlogDp) of 200 cm^{-3} at 2 microns aerodynamic diameter, and 60% of those particles from LSA.

The combined record of winds and particle size distributions was inspected to check for consistency with previous LSA work. A data filter was added to identify times with a high probability of identifying LSA. This used onshore wind directions (10° to 170°) and high wind speeds (> 4 m/s) and is represented by the blue shading in Fig 11. Not used in the filter, but shown as an independent variable in Fig 11 is buoy-measured wave height at Wilmette Buoy, IL. The wave break events often began after 10:00 am CST with the exception of June 5, 6, 7, and 14 where they began before 8:00 am CST and were sustained for several hours on average. During the event time periods, wave heights above 1 m occurred on June 5, 6, and 20 and onshore wind direction was from the northeast in all three cases. On June 6 number and volume concentrations remained relatively unchanged prior, during, and after the event and both concentrations decreased during and after the events on June 5 and 6.

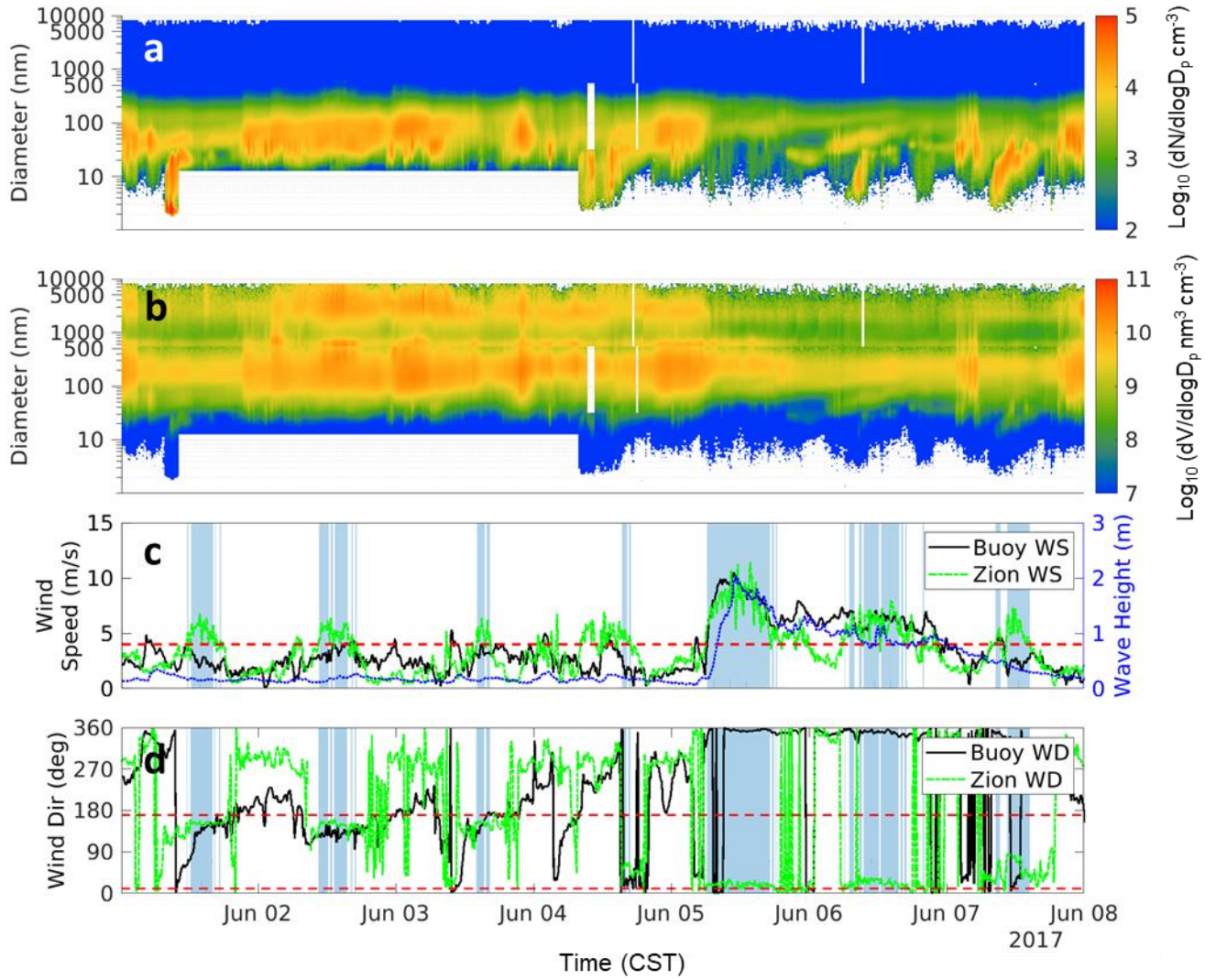

Fig 11. June 1- June 7 of 10 min PSD (a) and VSD (b); buoy windspeed (black), Zion windspeed (green), and wave height (blue) (c); buoy (black) and Zion wind direction (green) (d). Blue shaded region represents where Zion windspeed > 4 m/s and Zion wind direction between 10° and 170°.

The June 5 event was selected as the best candidate to observe potential LSA influence on the PSD for several reasons. First, wind direction was consistent from the north to northeast which likely reduces the influence of urban air plumes from the southern coast of the lake. Second, wave height above 1 m was sustained for several hours and peaked at 2 m, the highest recorded height during the campaign. Finally, it was the longest event during the campaign

lasting from 6:00 am to 5:00 pm CST. The PSD function was averaged for 2 hours prior, during, and 2 hours post event (Fig 12). The amplitude of the PSD function ($dN/dlogD_p$) from 9000 cm^{-3} prior to the event to 3000 cm^{-3} during and after the event and similar trend is observed in the volume distributions (not shown). During the event the number distribution mode was 81 nm and is in agreement with the first mode (80 nm) of the synthetic freshwater reported in May et al. [17] and Harb et al. [43].

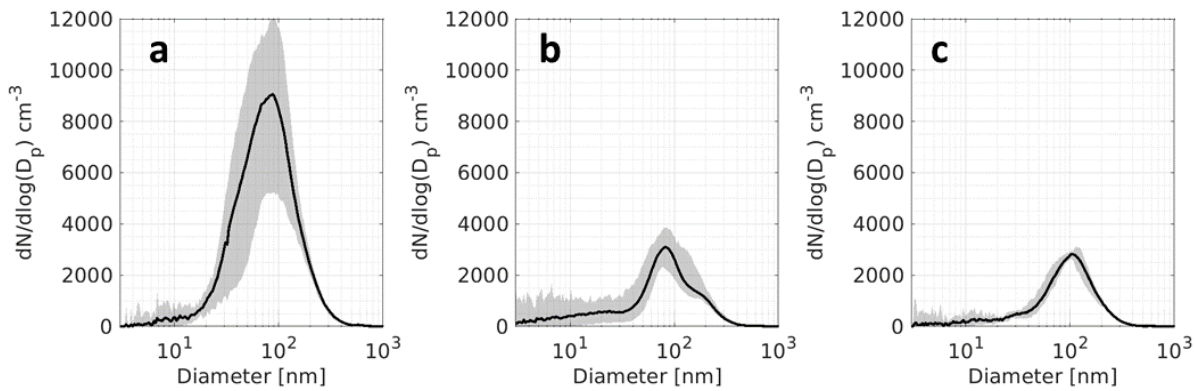

Fig 12. Arithmetic mean of PSD on June 5 for 2 hours prior (a), during (b), and 2 hours post (c) identified wave breaking conditions. Gray shaded regions represent 5th – 95th percentiles.

Additional exploratory analysis with the PSD, wind speeds, and wind direction was conducted. Periods with enhanced 30 and 80 modes were identified and it was seen if the occurrence of those modes, or their temporal variation in strength and mode position, were correlated with higher (> 4 m/s) velocity onshore flows. However, ultrafine particles seemed to occur during both higher velocity (> 4 m/s) and lower velocity (< 4 m/s) onshore flows, with variability not correlated with wind speed. Periods of high velocity (>4 m/s) onshore flow were identified and it was seen if the aerosol size distribution was noticeably different during these

periods. No consistent patterns emerged. Variations in the size distribution were, upon visible inspection, better correlated with variation in NO_x, isoprene, and MVK.

Finally, the period at the end of lake breeze days where the wind calmed but remained onshore was investigated. It was common for onshore flows to occur during the day, reaching velocities in excess of 4 m/s (sometimes up to 10 m/s), and then for wind speed to decrease in late afternoon, to speeds less than 4 m/s. We used this to see if there was an easily apparent (by visual inspection) pattern in the aerosol size distribution corresponding to this decrease in wind speed while offshore flow was maintained. This pattern occurred on June 1, 2, 3, 4, 8, 9, 11, 12, 13, 15, and 16, usually occurring at sunset. On June 2, 4, 8, and 16 there are visible decreases in sub 40 nm particles that correspond to the lowering of wind velocity, but in each case, causal inference is difficult. Slackening of the wind is (in these cases) often also correlated with decreases in NO_x and/or with evening growth of the ultrafine mode from condensation (ozone and SOA are often high at these times) and coagulation, giving an apparent decrease in sub 40 nm particles. On June 13, there is an increase in onshore wind speeds to over 4 m/s at about noon, and bursts of 10 nm particles associated with the wind gusts. However, these are coincident with increases in MVK and thus attribution to lake spray is doubtful.

In summary, LSA aerosols were not easily apparent during LMOS 2017, through examination of wind speed, wind direction, wave height, and measured PSD. However, considering the expected impacts on size-resolved number, total number, and mass compared to other sources of variability, our “negative detection” of LSA is likely consistent with the expected impacts, particularly those with lower absolute magnitudes. For example, impacts such as those reported by Chung et al. [23] (~100-250 cm^{-3} impact on aerosol number at shoreline sites), May et al. [41] (<1 μg m^{-3} of fine mode LSA aerosol), Amiri-Farahani et al. [24] (~5%

increase to PM over land), and Olson et al. [42] (modest elevation of the number distribution at 0.2 and 0.5 micron sizes) would be difficult to isolate from the LMOS 2017 record. The larger magnitude results, such as Slade et al. (1000-3000 cm^{-3} ultrafine particles under conditions of 2 m breaking waves) were not observed during LMOS 2017, despite having a period of onshore flow and 2 m breaking waves.

Spatial Context and Air Quality Implications

During LMOS 2017, the $PM_{2.5}$ concentration at Zion had mean values of 5.2 μg m^{-3} (filters) and 6.4 μg m^{-3} (reconstructed from PSD), with a standard deviation (at 2-min time resolution) of 4.3 μg m^{-3}. These are likely representative of urban-influenced background sites of the Great Lakes. These compare favorably to current US air quality standards (15 μg m^{-3}, annual $PM_{2.5}$; 35 μg m^{-3} daily $PM_{2.5}$), but are over the WHO guideline of 5 μg m^{-3}. Spatial variability of $PM_{2.5}$ was not resolved through observations during LMOS 2017 except through variation in particle concentration with the wind direction, and consideration of emissions from known sources [8]. We have shown through conditional probability analysis that particle concentrations of all sizes were, at Zion, more prevalent from sources to the west and in lake breezes originating to the southeast. Strong near-field $PM_{2.5}$ influences were shown to be limited in Doak et al. (2021), thus supporting spatial homogeneity of PM at approximately the 4 km distance.

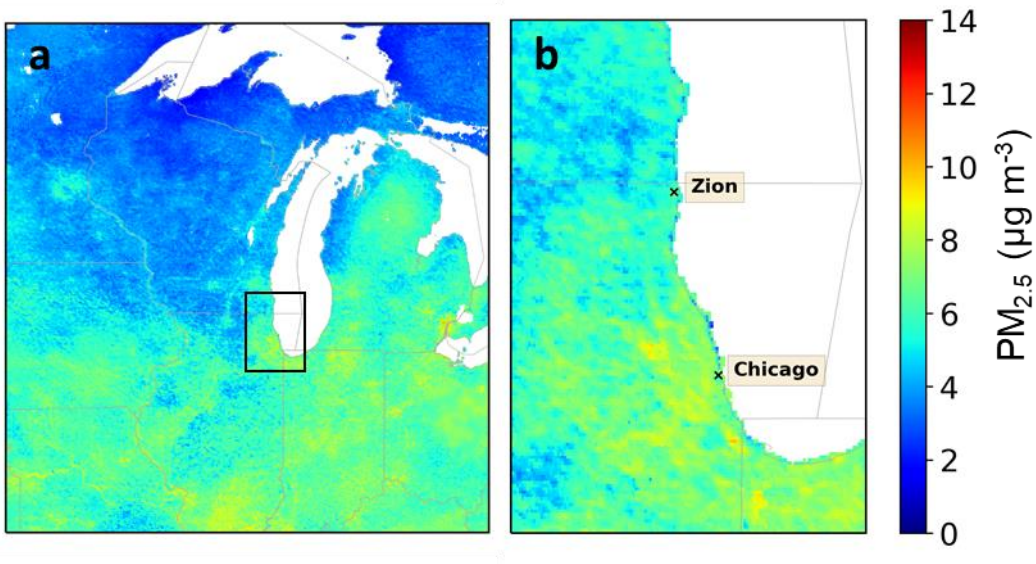

Fig 13. Estimated mean $PM_{2.5}$ for June 2017 for upper US Midwest (a) and southwest shore of Lake Michigan (b) as determined by combining AOD satellite retrievals with GEOS-Chem and calibrated with ground observations using geographically weighted regression [26].

The estimated mean $PM_{2.5}$ concentrations (spatial resolution of 1 km^2) in Fig 13 highlights moderate variation domain wide of 2 – 11 μg m^{-3} with the higher concentrations in the urban areas around the southern Great Lakes (Lake Erie and Lake Michigan). This also supports the higher concentrations of $PM_{2.5}$, ranging from 7-10 μg m^{-3} around the southwestern coast of Lake Michigan and the Zion average was estimated to be 6 μg m^{-3}. $PM_{2.5}$ is not estimated over the Great Lakes, not allowing for discussion of LSA or other aerosol sources over water.

However, NO_2 was measured with fine spatial resolution during LMOS 2017, using GeoTASO (spatial resolution of 250 m x 250 m) [44]. Furthermore, NO_x and $PM_{2.5}$ were correlated at Zion with a slope of 0.61 μg m^{-3} per ppb of NO_x and a coefficient of determination (R^2) of 0.51. Thus, pseudo-$PM_{2.5}$ mapping may be feasible (or downscaling of existing modeled or satellite-model-surface observation fusion) may be possible using NO_2 remote sensing.

Collocated $PM_{2.5}$ and NO_2 are available at several sites in the region and could be used to further assess the viability of downscaling $PM_{2.5}$ to detect hotspots over current or future standards. Several machine learning algorithms and regression modeling have supported that the relationship between $PM_{2.5}$ and co-pollutants (NO_2, SO_2, O_3) are important variables to consider when estimating $PM_{2.5}$ concentrations at high spatio-temporal resolutions and implications to epidemiological studies [45-47]. These methods are expected to continue to improve with the addition of geo-stationary satellites (TEMPO, GEMS) which will provide more temporally resolved data products.

Summary and Conclusions

Two SMPSs, a CPC, and an APS were deployed at Zion, IL in the summer during the LMOS 2017 field campaign. They provided a highly time-resolved particle size distribution in the range of 1.02 nm to 8.671 µm. The quality assured dataset was made publicly available for use in interpreting the particle size distributions, reconstructed PM concentrations, and future model-measurement comparisons; to the best of the authors' knowledge, few full size distribution datasets exist in the region.

The high index of agreement (0.83) and correlation (R = 0.90) of the independent CPC total number concentration (5783 cm^{-3}) supports the quality of the PSD number concentration (8485 cm^{-3}). The data quality is further supported by the favorable comparison in the overlap region of the two SMPSs, with an overall correlation (R = 0.90). Under 16 nm the 1 nm SMPS did measure consistently higher number concentrations with a 5:1 ratio. Zion number, surface area, and volume distribution modes and mean number concentrations, $N_{3\text{-}2500}$, are comparable to another rural Midwest site with urban influence (Bondville, IL). The number distribution was

dominated by ultrafine particles (mode = 40 nm) which is consistent with the mean AOD_{380} being a factor of 1.8 higher than AOD_{550}.

The PM mass was reconstructed from the PSD using an average particle density determined from the collocated gravimetric filters at the site. Intercomparison of $PM_{2.5}$ mass from the gravimetric filters, reconstructed PM, and nearby Chiwaukee Prairie are in agreement with correlations above 0.85, with the reconstructed mass being only 6.7% higher than the gravimetric mass, on average. On average, the PM_{10} was dominated by fine particulate, $PM_{2.5}$, as PM_{10} mass concentrations were only 1.5 µg m^{-3} higher than $PM_{2.5}$. AOD_{550} values rarely exceeded 0.2 and averaged 0.080 which is considered average clean conditions.

Very few conventional new particle formation events were detected during the campaign. This is partially due to the low concentrations and uptime of the 1 nm SMPS. Rather bursts of ultrafine particles were identified originating in the 3-10 nm size range. There was not clear evidence of LSA impact at the Zion site; however, this may be a signal-to-noise issue, as expectations based on previous modeling indicates minor enhancements due to LSA. Future confirmation of LSA aerosols should focus on (a) more northerly sites with lower anthropogenic influence, (b) chemical composition and microscopy at the size ranges of interest, and (c) vertical profiles from aircraft with simultaneous surface monitoring on shore. Sites should be located immediately at the shoreline rather than 100s of meters inland. Finally, LSA investigations may be able to leverage decrease in wind speed and wave activity but continued onshore wind direction at sunset during summer.

Supporting Information

S1 Table. A summary of local and NARSTO flags used on instrumental data for quality assurance during the campaign.

S2 Table. Statistics for particle variables measured during the LMOS campaign.

S1 Fig. Selected gas phase and aerosol variables for June 1 – 7, 2017 averaged to 10 min (except AOD). Timeseries of the particle size distribution in panel a, AOD_{380} (blue dot), AOD_{550} (purple dot), $PM_{2.5}$ (black), and PM_{10} (green) in panel b, total CPC number concentration in panel c, and NO_x (blue) and ozone (orange) in panel d.

S2 Fig. Hourly $PM_{2.5}$ from Chiwaukee Prairie from June 1 – 8, 2017.

S3 Fig. Same as S1 Fig. for June 8 – 15, 2017.

S4 Fig. Hourly $PM_{2.5}$ from Chiwaukee Prairie from June 8 – 15, 2017.

S5 Fig. June 8 – 15, 2017 of 10 min PSD (a) and VSD (b); buoy windspeed (black), Zion windspeed (green), and wave height (blue) (c); buoy (black) and Zion wind direction (green) (d). Blue shaded region represents where Zion windspeed > 4 m/s and Zion wind direction between 10° and 170°.

S6 Fig. Same as S1 Fig. for June 15 – 22, 2017.

S7 Fig. Hourly $PM_{2.5}$ from Chiwaukee Prairie from June 15 – 22, 2017.

S8 Fig. The same as S5 Fig. for June 15 – 22, 2017.

Acknowledgements

We acknowledge the entire LMOS Science Team, especially those involved with onsite measurements at Zion. Nathan Janechek and Nathan Bryngelson, of the University of Iowa, provided operational and maintenance assistance with many of the instruments used in this paper, and we thank them for their contribution.

Author Contributions

Conceptualization: COS, EAS, MBC. Data Curation: MBC. Formal Analysis: MBC, COS. Software: MBC, COS. Supervision: COS, EAS, RBP. Visualization: MBC. Funding Acquisition: COS, EAS, RBP. Writing – Original Draft Preparation: MBC, COS. Writing – Review and Editing: EAS, RBP, SE

References

1. Ramanathan V, Crutzen PJ, Kiehl JT, Rosenfeld D. Aerosols, Climate, and the Hydrological Cycle. Science. 2001 2001/12/07;294(5549):2119-24.

2. Watson JG. Visibility: Science and regulation. Journal of the Air & Waste Management Association. 2002;52(6):628-713.

3. Chen R, Hu B, Liu Y, Xu J, Yang G, Xu D, et al. Beyond PM2.5: The role of ultrafine particles on adverse health effects of air pollution. Biochimica et Biophysica Acta (BBA) - General Subjects. 2016 2016/12/01/;1860(12):2844-55.

4. Bari MA, Kindzierski WB. Fine particulate matter (PM2.5) in Edmonton, Canada: Source apportionment and potential risk for human health. Environmental Pollution. 2016 2016/11/01/;218:219-29.

5. Oberdörster G, Ferin J, Gelein R, Soderholm SC, Finkelstein J. Role of the alveolar macrophage in lung injury: studies with ultrafine particles. Environmental Health Perspectives. 1992;97:193-9.

6. Particles HRPoU. Understanding the Health Effects of Ambient Ultrafine Particles. Boston, MA: Health Effects Institute; 2013.

7. Stanier CO, Pierce RB, Abdi-Oskouei M, Adelman ZE, Al-Saadi J, Alwe HD, et al. Overview of the Lake Michigan Ozone Study 2017. Bulletin of the American Meteorological Society. 2021 25 Jun. 2021:1-47. English.

8. Doak AG, Christiansen MB, Alwe HD, Bertram TH, Carmichael G, Cleary P, et al. Characterization of ground-based atmospheric pollution and meteorology sampling stations during the Lake Michigan Ozone Study 2017. Journal of the Air & Waste Management Association. 2021:1-24.

9. Hughes DD, Christiansen MB, Milani A, Vermeuel MP, Novak GA, Alwe HD, et al. PM2.5 chemistry, organosulfates, and secondary organic aerosol during the 2017 Lake Michigan Ozone Study. Atmospheric Environment. 2021 2021/01/01/;244:117939.

10. Wagner TJ, Czarnetzki AC, Christiansen M, Pierce RB, Stanier CO, Dickens AF, et al. Observations of the Development and Vertical Structure of the Lake-Breeze Circulation during the 2017 Lake Michigan Ozone Study. Journal of the Atmospheric Sciences. 2022 01 Apr. 2022;79(4):1005-20. English.

11. Keeler GJ. Lake Michigan urban air toxics study. United States; 1994 1994-11-01.

12. Offenberg JH, Baker JE. Aerosol Size Distributions of Polycyclic Aromatic Hydrocarbons in Urban and Over-Water Atmospheres. Environmental Science & Technology. 1999 1999/10/01;33(19):3324-31.

13. Stolzenburg MR, McMurry PH. An Ultrafine Aerosol Condensation Nucleus Counter. Aerosol Science and Technology. 1991 1991/01/01;14(1):48-65.

14. Sipilä M, Lehtipalo K, Attoui M, Neitola K, Petäjä T, Aalto PP, et al. Laboratory Verification of PH-CPC's Ability to Monitor Atmospheric Sub-3 nm Clusters. Aerosol Science and Technology. 2009 2009/01/02;43(2):126-35.

15. Iida K, Stolzenburg MR, McMurry PH. Effect of Working Fluid on Sub-2 nm Particle Detection with a Laminar Flow Ultrafine Condensation Particle Counter. Aerosol Science and Technology. 2009;43(1):81-96.

16. Jiang J, Chen M, Kuang C, Attoui M, McMurry PH. Electrical Mobility Spectrometer Using a Diethylene Glycol Condensation Particle Counter for Measurement of Aerosol Size Distributions Down to 1 nm. Aerosol Science and Technology. 2011;45(4):510-21.

17. May NW, Axson JL, Watson A, Pratt KA, Ault AP. Lake spray aerosol generation: a method for producing representative particles from freshwater wave breaking. Atmospheric Measurement Techniques. 2016;9(9):4311-25.

18. Slade JH, VanReken TM, Mwaniki GR, Bertman S, Stirm B, Shepson PB. Aerosol production from the surface of the Great Lakes. Geophysical Research Letters. 2010 2010/09/01;37(18).

19. Song CH, Carmichael GR. A three-dimensional modeling investigation of the evolution processes of dust and sea-salt particles in east Asia. Journal of Geophysical Research: Atmospheres. 2001;106(D16):18131-54.

20. Schulz M, Leeuw Gd, Balkanski Y. Sea-salt aerosol source functions and emissions. Emissions of Atmospheric Trace Compounds: Springer; 2004. p. 333-59.

21. Barthel S, Tegen I, Wolke R. Do new sea spray aerosol source functions improve the results of a regional aerosol model? Atmospheric Environment. 2019;198:265-78.

22. Axson JL, May NW, Colón-Bernal ID, Pratt KA, Ault AP. Lake Spray Aerosol: A Chemical Signature from Individual Ambient Particles. Environmental Science & Technology. 2016 2016/09/20;50(18):9835-45.

23. Chung SH, Basarab BM, VanReken TM. Regional impacts of ultrafine particle emissions from the surface of the Great Lakes. Atmos Chem Phys. 2011;11(24):12601-15.

24. Amiri-Farahani A, Olson NE, Neubauer D, Roozitalab B, Ault AP, Steiner AL. Lake Spray Aerosol Emissions Alter Nitrogen Partitioning in the Great Lakes Region. Geophysical Research Letters. 2021 2021/06/28;48(12):e2021GL093727.

25. LMOS Team. LMOS- Lake Michigan Ozone Study 2017 2018 [Available from: https://www-air.larc.nasa.gov/missions/lmos/index.html.

26. van Donkelaar A, Hammer MS, Bindle L, Brauer M, Brook JR, Garay MJ, et al. Monthly Global Estimates of Fine Particulate Matter and Their Uncertainty. Environmental Science & Technology. 2021 2021/11/16;55(22):15287-300.

27. Bullard RL. Characterization of Nucleation and Ultrafine Particle Growth in Rural Continental Environments [Doctor of Philosphy]: Universit of Iowa; 2015.

28. Khlystov A, Stanier C, Pandis SN. An Algorithm for Combining Electrical Mobility and Aerodynamic Size Distributions Data when Measuring Ambient Aerosol Special Issue of Aerosol Science and Technology on Findings from the Fine Particulate Matter Supersites Program. Aerosol Science and Technology. 2004;38:229-38.

29. Bullard RL. Characterization of Nucleation and Ultrafine Particle Growth in Rural Continental Environments. 2015. p. 227.

30. Pettibone AJ. Toward a better understanding of new particle formation [Ph.D.]. Ann Arbor: The University of Iowa; 2009.

31. Downard J, Singh A, Bullard R, Jayarathne T, Rathnayake CM, Simmons DL, et al. Uncontrolled combustion of shredded tires in a landfill–Part 1: Characterization of gaseous and particulate emissions. Atmospheric Environment. 2015;104:195-204.

32. Lee BP, Li YJ, Flagan RC, Lo C, Chan CK. Sizing Characterization of the Fast-Mobility Particle Sizer (FMPS) Against SMPS and HR-ToF-AMS. Aerosol Science and Technology. 2013 2013/09/01;47(9):1030-7.

33. Bullard RL, Singh A, Anderson SM, Lehmann CMB, Stanier CO. 10-Month characterization of the aerosol number size distribution and related air quality and meteorology at the Bondville, IL Midwestern background site. Atmospheric Environment. 2017 2017/04/01/;154:348-61.

34. Kanawade VP, Benson DR, Lee S-H. Statistical analysis of 4-year observations of aerosol sizes in a semi-rural continental environment. Atmospheric Environment. 2012 2012/11/01/;59:30-8.

35. Stolzenburg MR, Scheckman JHT, Attoui M, Han H-S, McMurry PH. Characterization of the TSI model 3086 differential mobility analyzer for classifying aerosols down to 1 nm. Aerosol Science and Technology. 2018 2018/07/03;52(7):748-56.

36. Jiang J, Zhao J, Chen M, Eisele FL, Scheckman J, Williams BJ, et al. First Measurements of Neutral Atmospheric Cluster and 1–2 nm Particle Number Size Distributions During Nucleation Events. Aerosol Science and Technology. 2011 2011/03/10;45(4):ii-v.

37. Kontkanen J, Lehtipalo K, Ahonen L, Kangasluoma J, Manninen HE, Hakala J, et al. Measurements of sub-3 nm particles using a particle size magnifier in different environments: from clean mountain top to polluted megacities. Atmos Chem Phys. 2017;17(3):2163-87.

38. Kangasluoma J, Cai R, Jiang J, Deng C, Stolzenburg D, Ahonen LR, et al. Overview of measurements and current instrumentation for 1–10 nm aerosol particle number size distributions. Journal of Aerosol Science. 2020 2020/10/01/;148:105584.

39. Kulmala M. How Particles Nucleate and Grow. Science. 2003;302:1000-1.

40. Hussein T, Junninen H, Tunved P, Kristensson A, Dal Maso M, Riipinen I, et al. Time span and spatial scale of regional new particle formation events over Finland and Southern Sweden. Atmospheric Chemistry and Physics. 2009;9(14):4699-716.

41. May NW, Gunsch MJ, Olson NE, Bondy AL, Kirpes RM, Bertman SB, et al. Unexpected contributions of sea spray and lake spray aerosol to inland particulate matter. Environmental Science & Technology Letters. 2018;5(7):405-12.

42. Olson NE, May NW, Kirpes RM, Watson AE, Hajny KD, Slade JH, et al. Lake spray aerosol incorporated into Great Lakes clouds. ACS Earth and Space Chemistry. 2019;3(12):2765-74.

43. Harb C, Foroutan H. Experimental development of a lake spray source function and its model implementation for Great Lakes surface emissions. Atmos Chem Phys Discuss. 2022;2022:1-32.

44. Judd LM, Al-Saadi JA, Janz SJ, Kowalewski MG, Bradley Pierce R, Szykman JJ, et al. Evaluating the impact of spatial resolution on tropospheric NO2 column comparisons within urban areas using high-resolution airborne data. 2019:1-25.

45. Di Q, Amini H, Shi L, Kloog I, Silvern R, Kelly J, et al. An ensemble-based model of PM2.5 concentration across the contiguous United States with high spatiotemporal resolution. Environment International. 2019 2019/09/01/;130:104909.

46. Wong P-Y, Lee H-Y, Chen Y-C, Zeng Y-T, Chern Y-R, Chen N-T, et al. Using a land use regression model with machine learning to estimate ground level PM2.5. Environmental Pollution. 2021 2021/05/15/;277:116846.

47. Stafoggia M, Johansson C, Glantz P, Renzi M, Shtein A, de Hoogh K, et al. A Random Forest Approach to Estimate Daily Particulate Matter, Nitrogen Dioxide, and Ozone at Fine Spatial Resolution in Sweden. Atmosphere [Internet]. 2020; 11(3).

Supplemental Information

S1 Table. A summary of local and NARSTO flags used on instrumental data for quality assurance during the campaign.

Local Flag	NARSTO Flag	Description
DRY	M2	Diffusion dryer and drierite tube change
FLO	M2	Flow tests
DRN	M2	CPC water drain
INL	M2	Not sampling through inlet
HEP	M2	Leak check with HEPA filter
RHP	M2	RH probe check
STA	M2	Sampling trailer air
NET	V6	Neutralizers switched (x-ray and Kr-35)
TRB	M2	Troubleshooting instrument
UNK	M2	Unusual high counts
PUM	M2	CO2 pump not functioning
CAL	M2	SO2 span check with calibration gas
ZER	M2	SO2 zero test with zero air generator

S2 Table. Statistics for particle variables measured during the campaign

Variable	Time Avg (min)	Units	N	Mean	Std Dev	Min	5th	Median	95th	Max
$PM_{2.5}$	2	µg m^{-3}	18575	6.4	4.0	1.1	1.9	5.2	14.1	23.6
PM_{10}	2	µg m^{-3}	18575	7.9	5.0	1.3	2.3	6.6	16.9	37.7
CPC	2	cm^{-3}	15564	5,783	3,521	732	1,278	5,124	12,056	44,259
PN_p(3 – 8671 nm)*	2	cm^{-3}	8787	8,485	5,616	1,020	1,717	7,637	18,145	1.19×10^5
PN (1 – 3 nm)	2	cm^{-3}	14964	1.80×10^4	1.64×10^5	0	0	0	7,957	8.261×10^6
PN (3 – 10 nm)	2	cm^{-3}	14964	1,108	2,804	0	0	268	4,663	1.141×10^5
PN (10 – 500 nm)	2	cm^{-3}	13126	6,895	4,623	781	1,572	5,938	13,126	5.348×10^4
PN (3 – 2168 nm)	2	cm^{-3}	13126	7,993	5,919	783	1,608	6,835	1.79×10^4	1.191×10^5
PN (3 – 8671nm)	2	cm^{-3}	13126	7,998	5,921	783	1,608	6,836	1.79×10^4	1.191×10^5
PV (3 - 2168 nm)	2	µm^3 cm^{-3}	18575	4.78	2.99	0.83	1.44	3.90	10.60	17.73
PV (3 – 8671nm)	2	µm^3 cm^{-3}	18575	5.97	3.74	0.95	1.76	4.94	12.72	28.37
AOD_{550}	NA	unitless	404	0.084	0.0511	0.021	0.026	0.074	0.183	0.249

* statistics for June 1 – 21, 2017 for more direct comparison to CPC concentrations.

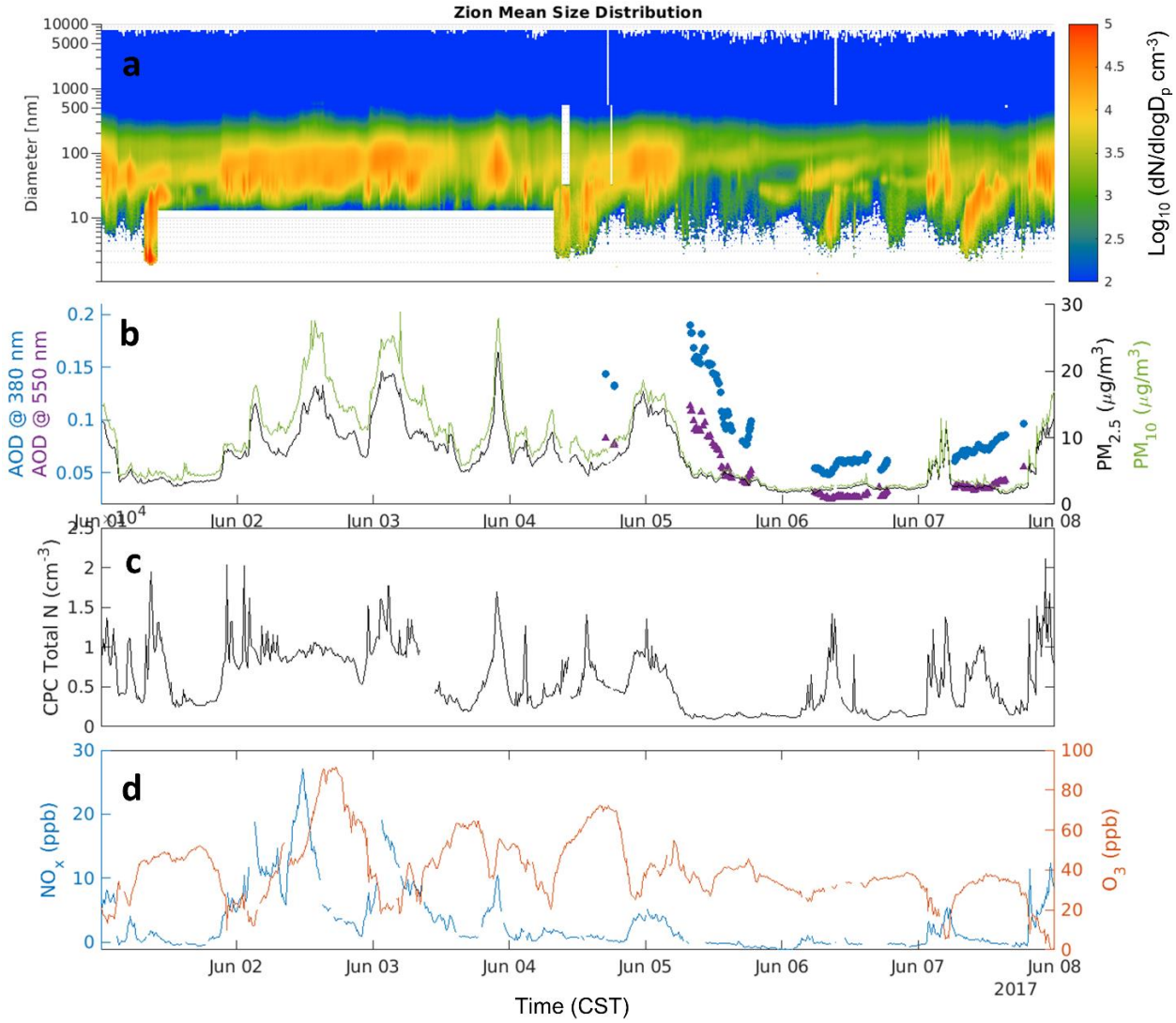

S1 Fig. Selected gas phase and aerosol variables for June 1 – 7, 2017 averaged to 10 min (except AOD). Timeseries of the particle size distribution in panel a, AOD_{380} (blue dot), AOD_{550} (purple dot), $PM_{2.5}$ (black), and PM_{10} (green) in panel b, total CPC number concentration in panel c, and NO_x (blue) and ozone (orange) in panel d.

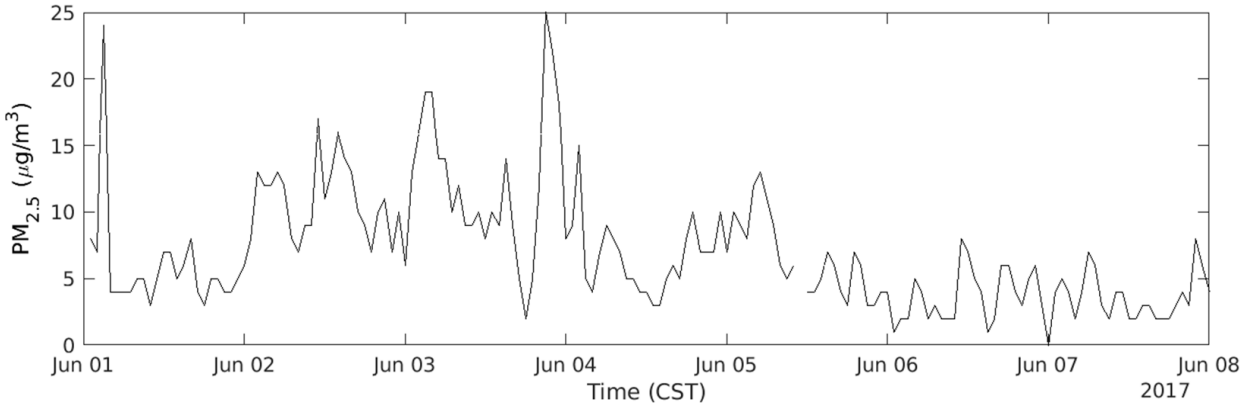

S2 Fig. Hourly $PM_{2.5}$ from Chiwaukee Prairie from June 1 – 8, 2017.

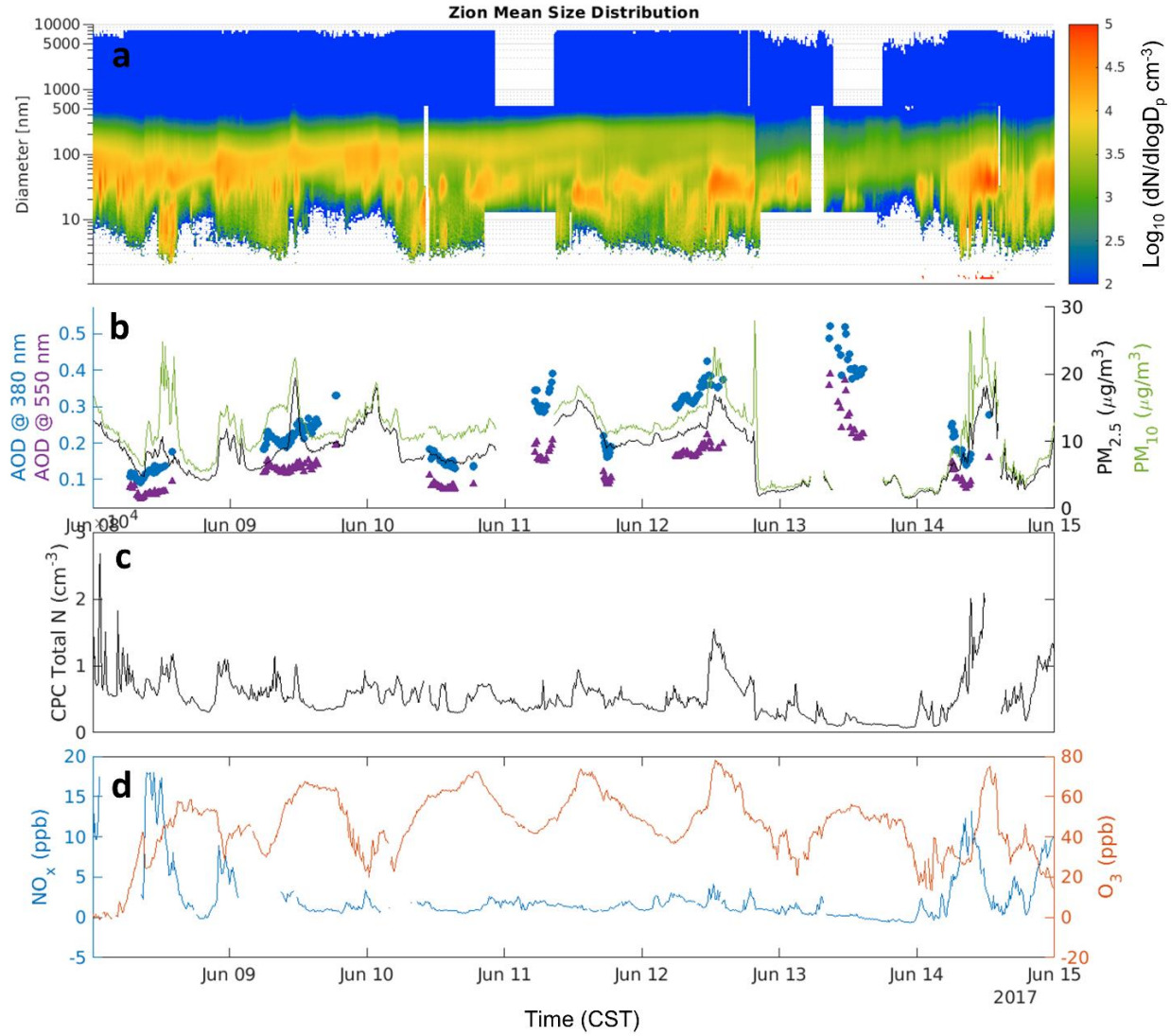

S3 Fig. Same as S1 Fig for June 8 – 15, 2017.

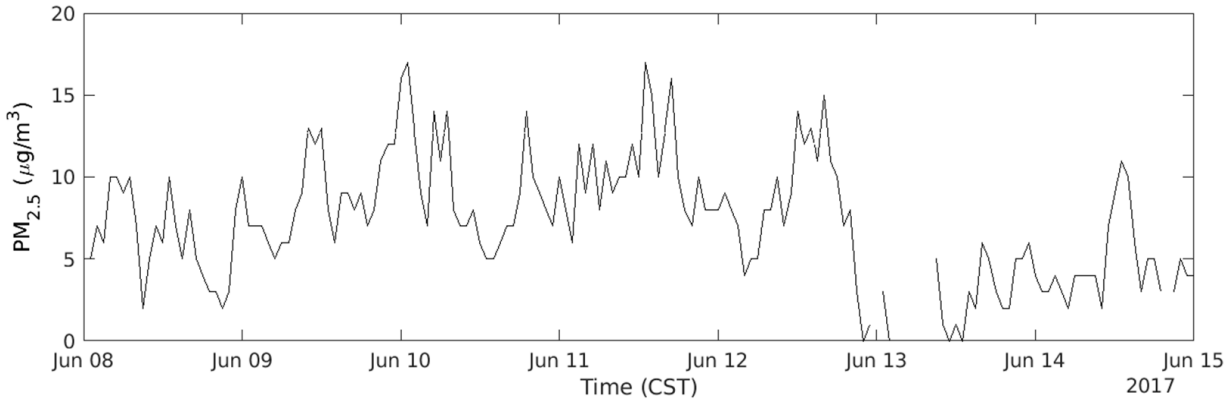

S4 Fig. Hourly $PM_{2.5}$ from Chiwaukee Prairie from June 8 – 15, 2017.

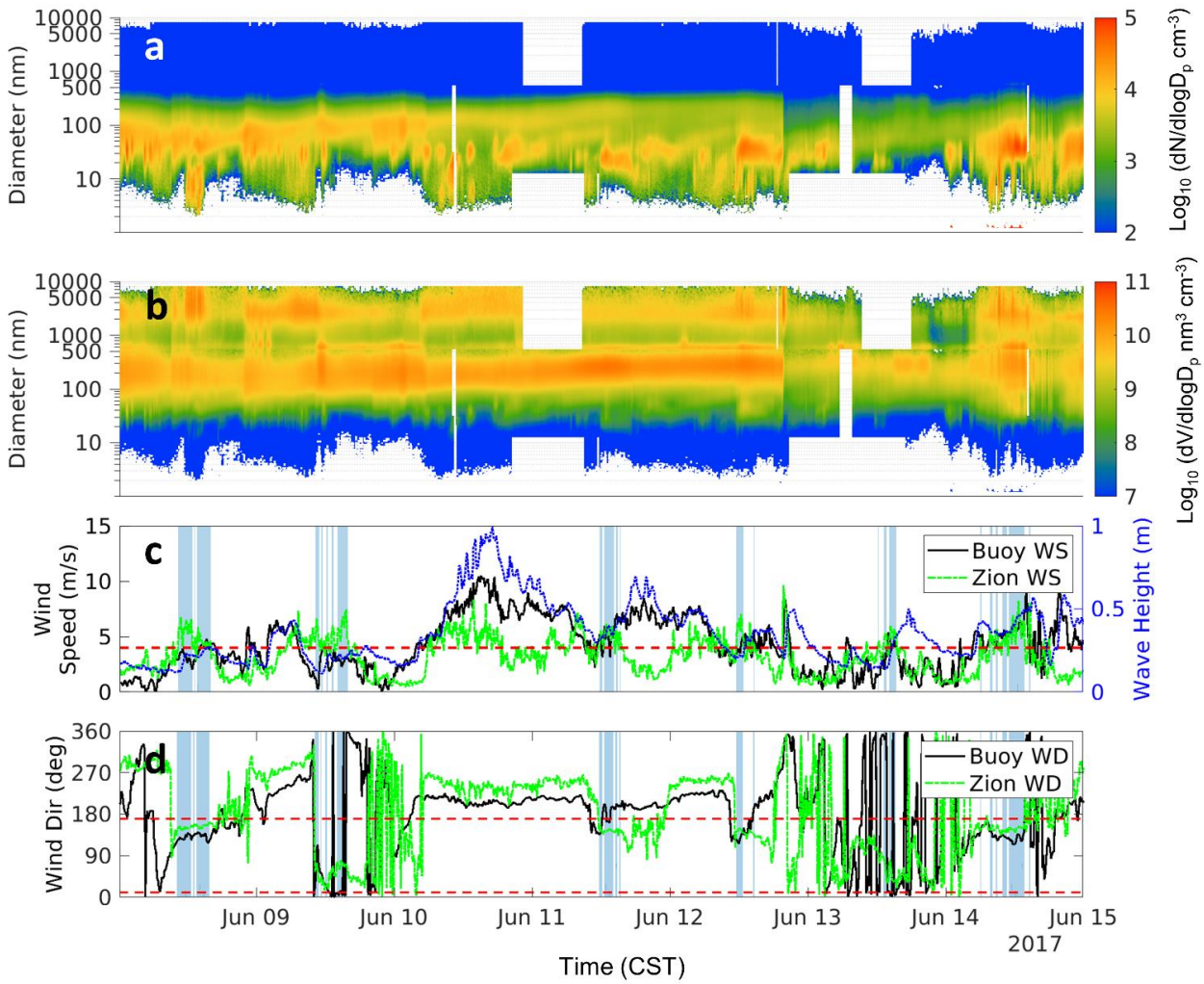

S5 Fig. June 8 – 15, 2017 of 10 min PSD (a) and VSD (b); buoy windspeed (black), Zion windspeed (green), and wave height (blue) (c); buoy (black) and Zion wind direction (green) (d). Blue shaded region represents where Zion windspeed > 4 m/s and Zion wind direction between 10° and 170°.

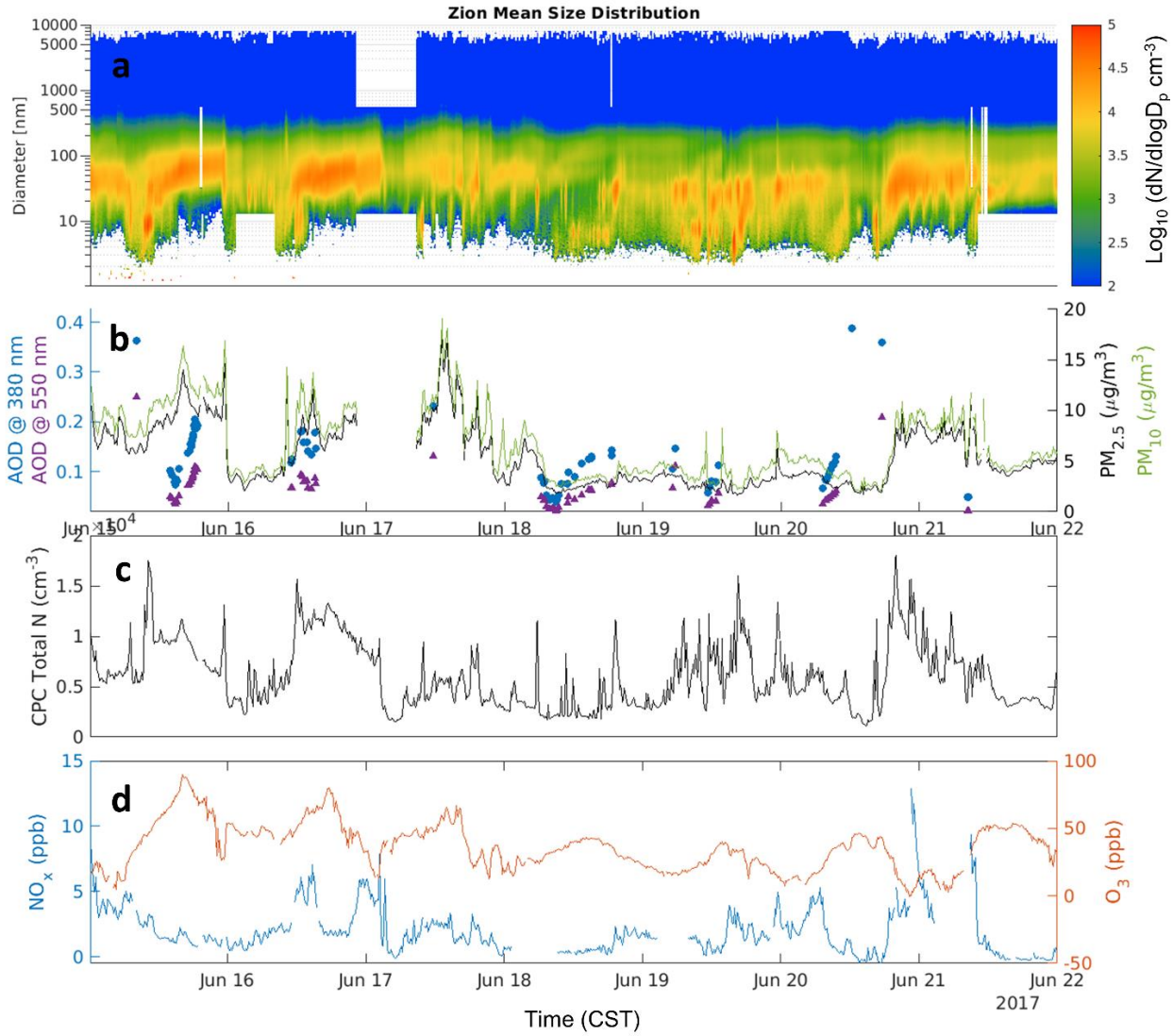

S6 Fig. Same as S1 Fig for June 15 – 22, 2017.

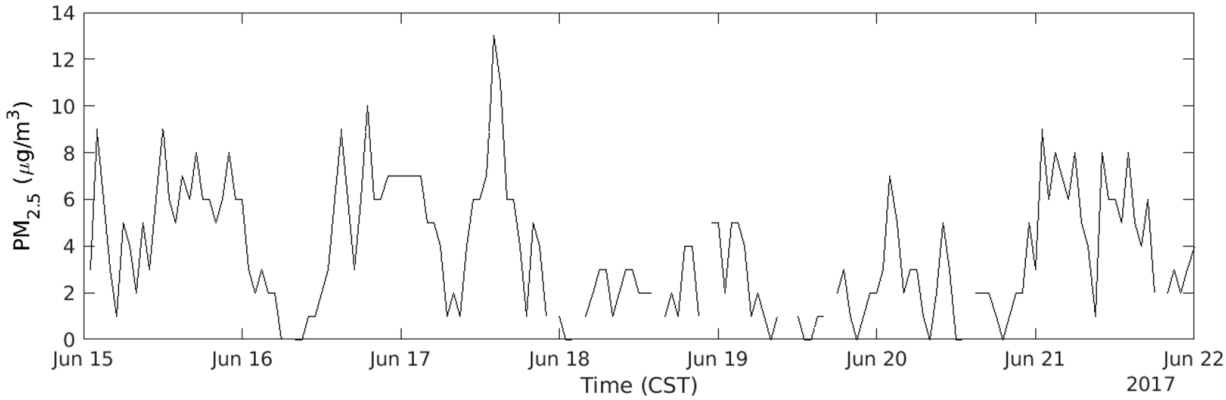

S7 Fig. Hourly $PM_{2.5}$ from Chiwaukee Prairie from June 15 – 22, 2017.

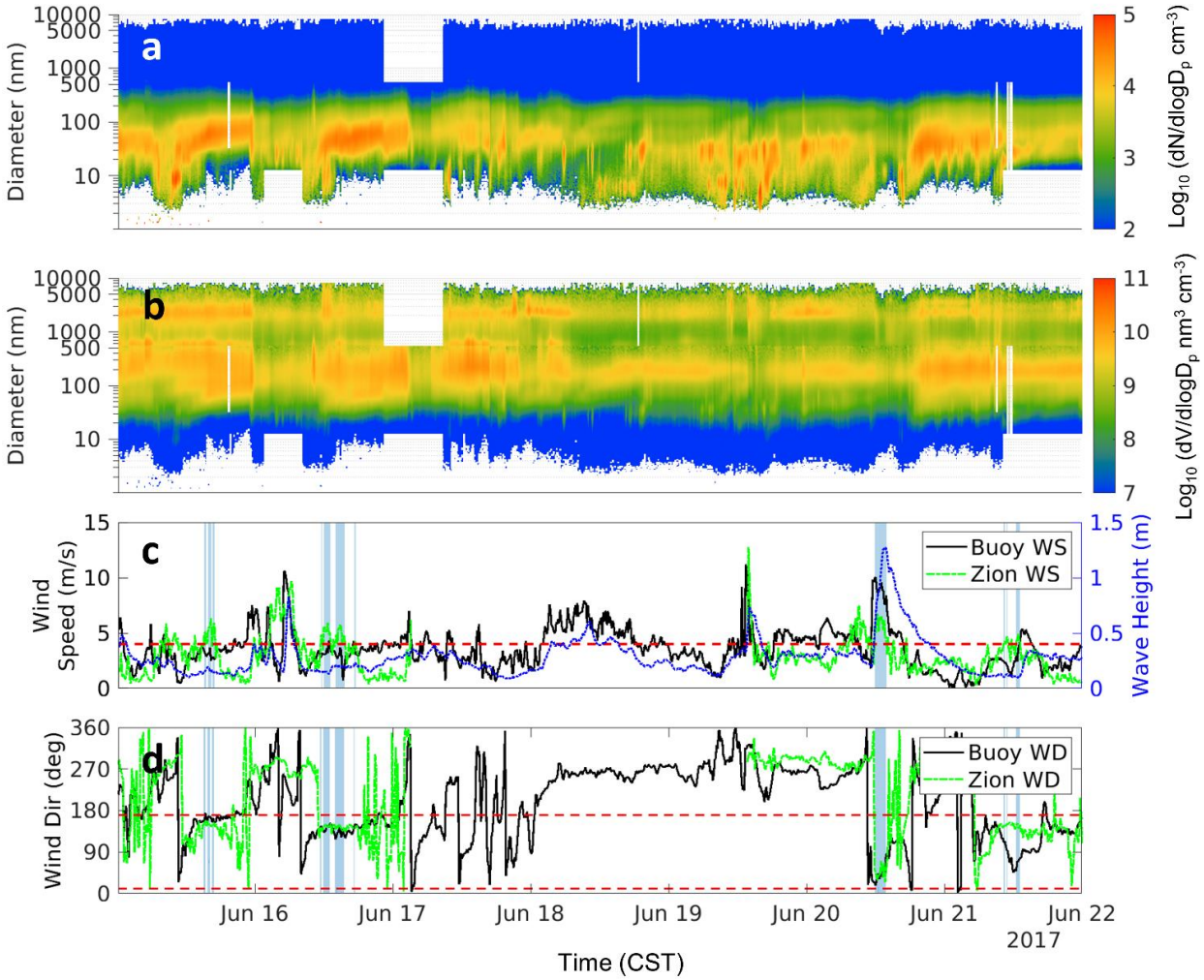

S8 Fig. The same as S5 Fig for June 15 – 22, 2017.